

Date of last edit: December 13, 2022

Scientific Project FluviMag: Fluvial Transport of Magnetominerals

Michael Pirrung

Dept. Applied Geology, Institute for Geosciences, Friedrich-Schiller University Jena,
Burgweg 11, D-07749 Jena, Germany, E-Mail: michael.pirrung@uni-jena.de

Thorsten Schäfer

Dept. Applied Geology, Institute for Geosciences, Friedrich-Schiller University Jena,
Burgweg 11, D-07749 Jena, Germany, E-Mail: thorsten.schaefer@uni-jena.de

Ioannis Paschalidis

Dept. of Chemistry, University of Cyprus. P. O. Box 20537, 1678 Nicosia, Cyprus, E-Mail:
pspasch@ucy.ac.cy

In July 2019 the authors, together with a group of students of the Master Program Geosciences of the University of Jena, had the opportunity to visit outcrops in the region of the Island of Cyprus that forms part of the European Union. Some field impressions of the Troodos Massif and its surroundings are presented in this manuscript together with new magnetic susceptibility data discussed in relation to published geochemical analyses and calculated normative mineral contents.

5.13. Crust-Mantle Transition at Troodos Massif, Cyprus

Starting a geological excursion at the highest part of Troodos Massif, located in the central southwestern part of the Island of Cyprus, means to get access to earth's mantle rocks. Descending the slopes of the massif provides an insight into the mantle to oceanic crust transition zone, further outwards several layers of the oceanic crust are exposed, and finally sediments cover the lowlands up to the coastline. The relatively undisturbed stratigraphic conditions of this ophiolite complex turn field studies on the island to an extraordinary experience. Many stops visited during the excursion have been selected from (EDWARDS, S., et al. 2010), including an extensive list of references, and from (ANONYMOUS 2018). Newer information about structural, petrographical and geochemical aspects is presented e.g. by (COOGAN, L.A. & GILLIS, K.M. 2018), (MCPHEE, P.J. & VAN HINSBERGEN, D.J.J. 2019), (OSOZAWA, S., et al. 2012). The central part of Troodos Massifs is protected as UNESCO Geopark, see www.troodos-geo.org, and no rock samples may be taken without special permission.

An impression of Troodos Massif rocks can be obtained at the Troodos Geopark Visitors' Centre at Pano Amiantos, see <https://www.visitsolea.com/troodos-geopark-visitors-centre/?lang=en>, where information about the ophiolite sequence, mineralogy, lithology and mining history is presented. In an outdoor area blocks of typical lithologies and fabrics can be studied macroscopically. This helps to assign a rock name to many rocks exposed in outcrops. Information on the remediation project in the former Amiantos Asbestos Mine in the centre of Troodos Massif, where mining activities ended in 1988 and remediation started in 2009, is given under <https://www.visitsolea.com/amiantos-asbestos-mine/?lang=en>,

<https://www.amiandos.eu/en/>. Floral and faunal features of Troodos National Forest Park are presented at the Visitor Centre at Troodos, see <http://www.troodos-geo.org/cgi-bin/hweb?-A=196&-V=troodos>.

We highly appreciate the permit of the Cyprus Geological Survey to take a limited amount and volume of samples to Germany. The total mass of rock samples analysed for this study was 260 g of own samples, supplemented were further samples of a petrological kit of Troodos Massif rocks kindly provided by the Cyprus Geological Survey, and samples purchased from a Cypriot collector.

In addition to magnetic susceptibility data measured in this study, a compilation of geochemical data was retrieved, for comparison of susceptibility values with normative magnetite content. To the opinion of the authors, in this manuscript the most expansive review of geochemical data of Troodos Ophiolite publicly accessible is presented.

[5.13.1. Short overview on the geology of Cyprus](#)

[5.13.2. Classification of magmatic rocks of Troodos Ophiolite](#)

[5.13.3. Petrogenesis of magmatic rocks of Troodos Ophiolite](#)

[5.13.4. Plate tectonic milieu interpreted from chemical analyses of Troodos Ophiolite](#)

[5.13.5. Magnetic susceptibility of whole rocks from Cyprus](#)

[5.13.6. Geochemistry and magnetic susceptibility](#)

[5.13.7. Summary and outlook](#)

[5.13.8. References](#)

5.13.1. Short overview on the geology of Cyprus

The Troodos Massif in the central to western part of the present island of Cyprus represents a part of oceanic lithosphere (EDWARDS, S., et al. 2010). It forms an ophiolite complex where oceanic crust has been uplifted. New, hot and light oceanic crust in general is formed under a distension regime at the mid-ocean ridges in seafloor spreading zones, also denoted as oceanic rift zones (FRISCH, W. & MESCHEDE, M. 2005). Usually older and cooler oceanic crust of higher density is subducted under lighter continental or relatively hot oceanic crust or an island arc under a compressional regime. The obduction of oceanic crust by thrusting onto oceanic or continental crust may occur if the compressional regime starts soon after the spreading when the oceanic crust is still relatively warm and thus too light to be subducted in a collisional zone. Such an obduction may be the consequence of a change in the stress regime by a new tectonic plate configuration. Since their obduction towards the north of the Cyprus Trench three microplates, Troodos in the center, Mamonia in the southwest and Cyrenia in the northeast, were accreted to the present island (EDWARDS, S., et al. 2010).

In the following paragraphs a short geological and petrographical characterisation of the lithostratigraphic units of Cyprus is given, followed by a brief summary of Mamonia and Cyrenia terrains, mainly based on (EDWARDS, S., et al. 2010).

The Troodos microplate consists of Upper Cretaceous oceanic lithosphere that was formed within a supra-subduction zone (EDWARDS, S., et al. 2010). Rocks are relatively undeformed and non- to epimetamorphic. Strong uplift of the central part with ultramafic mantle rocks, more or less altered to serpentine (HENRY, B. 1971), coincides with highest present elevations around Troodos Square. With increasing horizontal distance to this central part, gabbros, sheeted dykes, volcanics and deep water sediments form WNW-ESE-stretched elliptic bands with increasing diameter. In [table 5.13-1](#) an overview of the characteristics of ophiolite rocks of Troodos Massif is given. More information on petrology and geochemistry will be given in the following chapters. Economically interesting mineralisations are concentrated in ultramafic rocks, with chromite, FeCr_2O_4 , and asbestos, a group of several serpentine minerals, and in volcanic rocks, with sulfidic ores. In the south of the massif a transform fault situated under the Arakapas Valley separates the main part of the ophiolite from a smaller part in the Limassol Forest (EDWARDS, S., et al. 2010). Prehistoric ore mining places are concentrated in the volcanic sequence, as well as industrial mining sites of the 19th to 21st century. The wealth of exploitable ores, especially of copper, was a main reason for prospering antique settlements on the island, as e.g. at Kourion. For museums and archeological parks see information available under <http://www.mcw.gov.cy/mcw/da/da.nsf/All/21E14D80F55D8539C22571990020DC5C?OpenDocument>.

A counter-clockwise rotation of Troodos Massif of about 90° was the consequence of microplate movement under changing stress conditions (EDWARDS, S., et al. 2010) when the former Tethys Ocean was closed in the late Meso- to early Cenozoic era during alpine collision.

Mamonia terrain rocks consist of Triassic to Upper Cretaceous lavas covered by Mesozoic sediments, partly metamorphosed, tectonised with intermingled parts of Troodos lithosphere (EDWARDS, S., et al. 2010).

Cyrenia terrain sediments represent parts of Permian, Triassic and Jurassic shelf carbonates that were partly metamorphosed to form marbles and schists during Upper Cretaceous. Overlying sediments and volcanics of Upper Cretaceous to recent age are less deformed and were developed as a shallowing upwards sequence (EDWARDS, S., et al. 2010), pp.12-14. A major thrust towards the south is visible in the topography of northernmost Cyprus (EDWARDS, S., et al. 2010), in an area at present under Turkish administration.

Tab. 5.13-1: Overview on Upper Cretaceous Troodos ophiolite sequence from top to base according to (EDWARDS, S., et al. 2010), with some additional observations by (WIMMENAUER, W. 1985). Abbreviations: an = anorthite, cc = calcite, cpx = clinopyroxene, cr = chromite, ep = epidote, gy = gypsum, hem = hematite, kf = orthoclase, mt = magnetite, ol = olivine, opx = orthopyroxene, plag = plagioclase, pyr = pyroxene, ser = serpentine; XX = crystals; % as vol.-%; sec. = secondary. All mantle and plutonic rocks are holocrystalline, dolerites are holo- and microcrystalline, volcanics normally are porphyric with fine-grained matrix and phenocrysts or they are aphyric. Traditionally, the Volcanic Sequence was subdivided into the Basal Group, the Lower and the Upper Pillow Lavas. This was not applied in this table, for arguments see (EDWARDS, S., et al. 2010), pp. 73-75. From the Circum Troodos Sedimentary Sequence only those formations are presented here that were visited during our excursion. Sites: GP = site of Troodos Geopark, GPM = Mine of Troodos Geopark; ED = stop of (EDWARDS, S., et al. 2010).

Lithostratigraphical unit/Site	Rock type	Petrography	Texture	Interpretation
Circum Troodos Sedimentary Sequence	Recent beach sediments at Governors Beach and at Larnaca	Grey sands	Surprisingly low amount of shells	Mixture of eroded mafic and ultramafic rock debris with carbonate material
Circum Troodos Sedimentary Sequence	Litoral sediments at Larnaca Salt Lake [Pleistocene and recent]	Conglomerate of mafic pebbles in a calcareous sandy matrix; recent litoral algae and biofilms	Fossils of reef corals, shells of gastropods, bivalves, serpulids	Beachrock; proximal sediments of coastal lagoon
Circum Troodos Sedimentary Sequence	Nicosia Formation at Latouros Quarry [Pliocene]	Shell-rich sands, calcarenite	Almost no fine-grained siliciclastic matrix	Well-sorted carbonate sands on marine terrace, transgression after Messinian Event
Circum Troodos Sedimentary Sequence	Pakna Formation at Kouris Dam [Lower Miocene]	Chalks, lime- and marlstones	Sections of planar bedding contrast to wedges of folded bedding	Hemipelagic still-water sedimentation interrupted by slumps.
Circum Troodos Sedimentary Sequence	Lefkara Formation at Governors Beach [Paleocene to Oligocene]	Whitish chalk with deformed beige chert bands	Bioturbated carbonate sediments	Shallow-water deposition
Perapedhi Formation	Radiolarites, marlstones [Upper Cretaceous]	Cryptocrystalline silica, clay minerals	Not visited during our excursion	First deep-water sediments
Volcanic sequence	Ochre	Mixture of hydrated Fe-Oxides	Fine-grained, yellow to ochre, very low Mn-content	Submarine weathering of sulfides

Volcanic sequence	Umber	Metalliferous Fe- and Mn-oxides	Fine-grained, dark brown, red if altered to jasper, filling in depressions of pillow lavas	Precipitated at black smokers, jasper from feldspar alteration
Volcanic sequence	Sheetflows, hyaloclastites, pillow breccias	See above	Not visited during our excursion	
Volcanic sequence	Sulfidic ores	Pyrite, qz, sec. hem, gy	Massive dark ore bodies or dispersed sulfides in volcanic rocks, in oxidation zone reddish to yellowish colours	Exhalation of Fe-, Cu-, Zn-, Mn-rich fluids and precipitation at the seafloor at and around black smokers, upward movement branch of hydrothermal circulation, leaching of sulfides from sheeted dykes that subsequently become epidiosites
Volcanic sequence	Basaltic pillow lavas	Plag, pyr	Bulbous pillows 0.2-1 m in diameter with chilled margins and bubbles at center, fine-grained to aphyric, often some mafic XX, cc and qz veins	Final parts of lava tubes; veins of cc or qz and chilled margins from interaction with seawater
	“upper”			
	“lower”			
	“basal”			
Sheeted-dyke sequence	Dolerite “Diabase”	Similar to gabbro	Bluish-grey to brownish-green, medium- to coarse-grained, sometimes light plag-rich nests, rarely hypidiomorphic, no phenocrysts, ophitic = irregular plag XX within pyr, often plag replaced by qz+ep, finer margins of dykes	Multiple dyke intrusion at several kilometers depth, no host rocks other than dykes, sometimes intruded by younger basaltic dykes with chilled margins
Plutonic sequence	Plagiogranite	Qz, zoned plag with an <40 %, kf <5 %	Grey, fine- to medium-grained, plag often altered to epidote and then whitish colors, graphophyric intergrowth of plag with qz, few mafic XX	Late stage of fractionate crystallisation, top of magma chamber, intrusion into gabbros, restricted to oceanic crust
Plutonic sequence	Diorite	Like gabbro, but plag with an <50 %	See below	See below
Plutonic sequence	Gabbro	Plag with an ≥50 %, ol, pyr, sec. ep	Medium- to coarsegrained, <40 cm thick layering of different grainsize and mineral composition, foliation from high-temperature plastic deformation; sometimes pegmatitic	Layering of early crystallisates in lower part of magma chamber
Mantle sequence	Serpentinite	Ser, ±mt, cr	Greenish, mostly dense, sometimes relics of mafic XX with differing colours or luster, frequent slickensides, white bands of fibrous chrysotile asbestos without preferred orientation	Early high-temperature and late to recent low-temperature hydrothermal alteration of ultramafic rocks

Mantle sequence	Pyroxenite [ultramafic]	Ultramafic cumulates of ol, opx, cpx ≤ 40 % ol, ≥ 60 % opx+cpx, \pm cr	veins and lenses in harzburgite, foliation // to host rock	Transition of mantle to lowermost crust, fractionate crystallisation, partial melting of Wehrlite
Mantle sequence	Wehrlite [ultramafic, peridotite]	≥ 40 % ol, 10-60 % cpx, ≤ 5 % opx, \pm plag	Coarse-grained, brownish cumulate of subrounded ol surrounded by dark pyr, poikilitic plag within younger cpx	Intrusion into gabbros, pyr-generating melt intruded into dunite
Mantle sequence	Chromitite [ultramafic]	cr, ol	Medium-grained dark metallic black cr and yellowish-green ol, layers and veins in dunite	Fractionate crystallisation, melt-harzburgite-reaction with opx \rightarrow ol+cr
Mantle sequence	Dunite [ultramafic, peridotite]	≥ 90 % ol, \pm cr, cpx	Fine-grained, dark altered ol, veins and lenses in harzburgite, foliation // to host rock	Transition of mantle to lowermost crust, melt-harzburgite-interaction with ol as insoluble residuum of pyr or meltout of opx from harzburgite
Mantle sequence	Harzburgite [ultramafic, peridotite]	≥ 40 % ol, ≤ 40 % opx, ≤ 5 % cpx, \pm cr	Well-defined light-reflecting pyr XX and altered brownish ol, foliation from high-temperature plastic flow, layering from crystal settling	Ultrabasic residuum of magma chamber with partial melting of upper mantle lherzolite

The Circum-Troodos Sedimentary Sequence of Upper Cretaceous to recent age covers all three terrains. Northward underthrusting of African lithosphere under the Eurasian plate in the Cyprus Trench resulted in uplift of parts of the present island since Miocene (EDWARDS, S., et al. 2010), p. 14.

Geological maps of the entire Island of Cyprus or of parts of it have been published by the Cyprus Geological survey, see e.g. (PANTAZIS, T. 1979), links are given in the [references chapter](#), and by several further authors, see e.g. (EDWARDS, S., et al. 2010), p. 10, (REN, L., et al. 2015), geological profiles are shown by e.g. (DILEK, Y. & FURNES, H. 2009), (MCPHEE, P.J. & VAN HINSBERGEN, D.J.J. 2019). General schemes of the ophiolite sequence are shown by e.g. (EDWARDS, S., et al. 2010), p. 21, 25, 26; (DILEK, Y. & FURNES, H. 2009); schematic lithological profiles of the Circum Troodos Sedimentary Sequence are shown by (EDWARDS, S., et al. 2010) and (REN, L., et al. 2015). Links to top maps and ore mining sites are given in the references chapter.

The map in [figure 5.13-1](#) localises outcrops visited and partly sampled in July 2019 and also indicates some outcrops presented in [figure 5.13-2](#). The latter figure shows selected field impressions of rocks of Cyprus, a few photos of historic or technical buildings are included in addition.

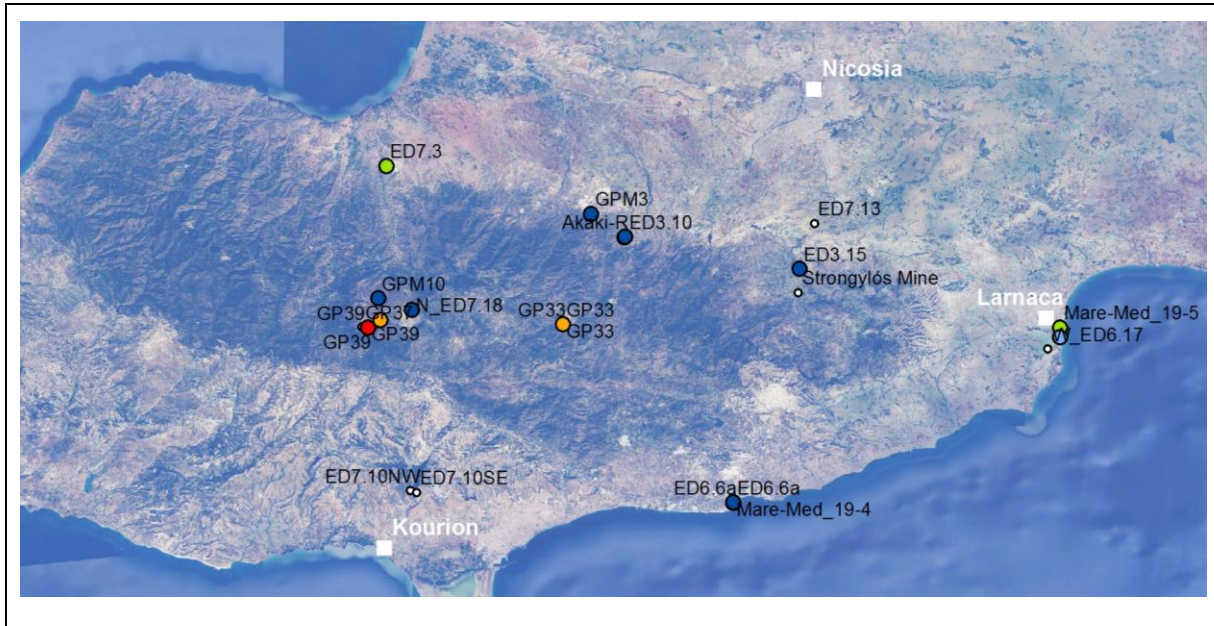
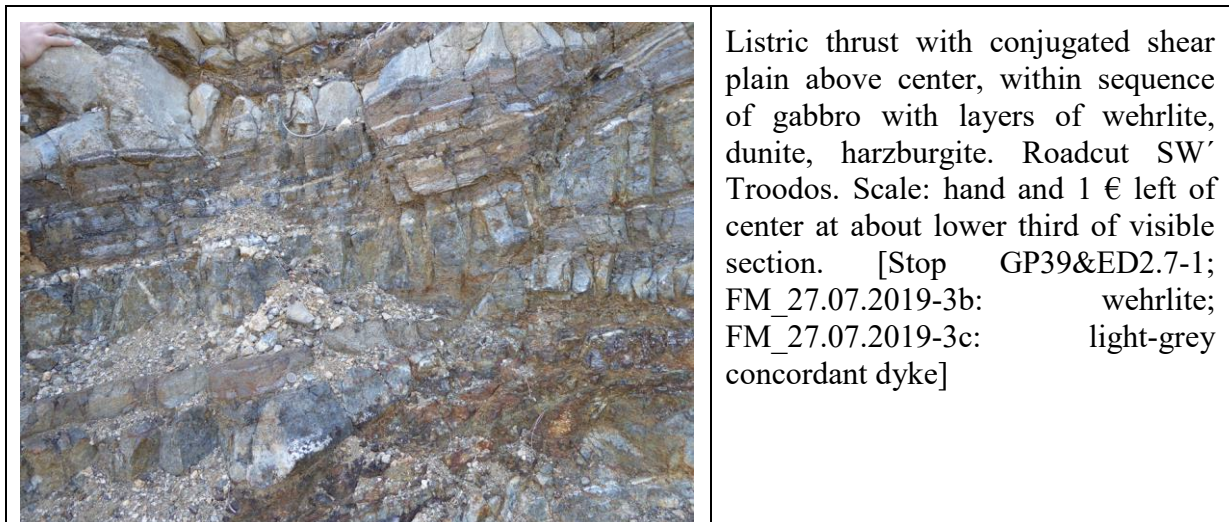


Fig. 5.13-1: Map of the central to southern part of the Island of Cyprus showing locations that were sampled, or are visualized in [fig. 5.13-2](#), during the excursion of the Department Applied Geology of the Friedrich-Schiller-University in 2019, supported by the University of Cyprus and the Cyprus Geological Survey. Few cities are inserted for orientation. Sites: GP = site of Troodos Geopark, GPM = Mine of Troodos Geopark; ED = stop of (EDWARDS, S., et al. 2010). Colors mark the quantity of mass-specific magnetic susceptibility determined on whole rock samples [$10^{-9} \text{ m}^3\text{kg}^{-1}$]: <100, 100-499, 500-999, 1000-10000, >10000. The ophiolite complex of Troodos Massif is clearly visible by the dark colors of forest and of mafic and ultramafic rocks. The map is based on aerial images © Google Earth.





Gabbro, grey, with ultramafic brownish layers, probably dunite, with conjugated shear plains right of center, fault-related breccia at center, extensional fault with curved geometry in the brown layer left of center. [Stop GP39& ED2.7-1]



Isoclinal fold in ultramafic rocks, supposedly of dunite and wehrlite. Such folds indicate plastic deformation under high temperatures within the lowermost part of a magma chamber, where cumulates of heavy crystals like olivine and ortho- and clinopyroxene form. [Stop GP39&ED2.7-1]



Homogenous medium-sized gabbro, apparently fresh and therefore probably a younger intrusion compared to surrounding ultramafic rocks; dark spots pyroxene, light spots feldspar, eventually also epidote. [Stop GP39&ED2.7-1; FM_27.07.2019-3a: see left]



Wehrlite in this variety is a coarse-grained peridotite, with brown olivine crystals surrounded by clino-pyroxenes, both are altered to serpentine. Tailing at viewpoint at bend north of Amiantos Asbestos Mine, to the NW of Kato Amiantos. [Stop GPM11&ED7.18]



Dark brown massive chromitite mainly consists of chromite = chrome spinel, FeCrO_4 , black, and olivine, grey. The density of this material is very high with 4.7 to 5.1 g cm^{-3} . Heap off the entrance of Kannoures Mine on the northern slope of Mt. Olympos. [Stop GPM10&ED2.3; FM 31.07.2019-2: pieces around coin]



Serpentinite resulted from hydrothermal alteration of ultramafic rocks like harzburgite within the oceanic crust. Since these rocks have a lower density compared to their parent rocks, their occurrence in the centre of the Troodos Ophiolite produces uplift. Steep slopes within serpentinite tend to be instable, evident from a land slide in a former open pit. Northern slope of Amiantos Asbestos Mine.



One of the goals of remediation strategy is the creation of stable slopes in former open pits, in order to reduce exposed areas of mined rocks. Locally this effort was counteracted by surface runoff during thunder storms and consecutive mass transport by slope wash processes. As a consequence a miniature alluvial fan has established. From its surface area wind can blow off fine particles. Northwestern slope of Amiantos Asbestos Mine.



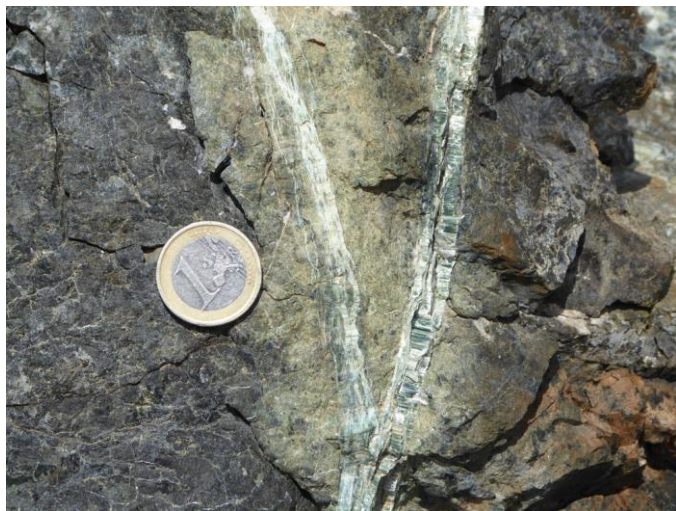
P1040284 Large crystals of serpentine, probably antigorite, in a matrix of white serpentine. Probably relictic fabric of coarse-grained ultramafite. [Between Stop GP37&ED2.7-2 and Stop GP39&ED2.7-1]



Green, brilliant, non-fibrous serpentine, ? Antigorite, with slickensides. Steps point to movement of former hanging rock part towards lower right. Pebble in valley north of entrance to Amiantos Asbestos Mine. [FM_Loumata-River2019-1: creek sediment; FM_27.07.2019-2: similar serpentinite, from Amiantos Asbestos Mine]



Dense, relatively homogeneous brownish serpentine with bands of white chrysotile asbestos. White fibres are probably low-thermal products, ? subrecent near-surface joint fillings resulting from uplift-related pressure release, within serpentinite. Irregular orientation of joints. Viewpoint at bend north of Amiantos Asbestos Mine. [Stop GPM11&ED7.18]



Transition of granular serpentinite into hydrothermally bleached serpentinite with fibrous greenish serpentinite, white bands of chrysotile. Amiantos Asbestos Mine, NW-part of publicly accessible area.



Fibrous and non-fibrous varieties of serpentine minerals are present as veins in dark brownish-green serpentinite. Most of the rocks were not suitable for extraction of chrysotile, therefore large heaps resulted from mining activities. Amiantos Asbestos Mine.



The tube-shaped structure of the serpentine mineral Chrysotile, $Mg_3Si_2O_5(OH)_4$, is expressed in the fibrous habit. Small particles are respirable and pose severe health problems. Until the 1990s serpentinite was used e.g. for isolation material in buildings. Amiantos Asbestos Mine.



Another product of hydrothermal alteration of ultramafic, Mg-rich, rocks is the mineral talc, $Mg_3 [OH_2 Si_4O_{10}]$. Talc belongs to the minerals with lowest hardness. Here the remains of a slickenside survived alteration. Pebble in the valley northeast of entrance to Amiantos Asbestos Mine.



Outcrops are part of the bastite-serpentinite breccia (HENRY, B. 1971), to which the serpentinites at Amiantos belong as well. Slopes are covered by debris upon which channels of rockfalls are visible. Lack of vegetation points to very active resedimentation processes, due to the recent uplift of and regressive erosion into Troodos Massif. View from the forest road descending from Troodos Square northwards to Kannoures Mine [Stop GPM10&ED2.3].



Dark fine-grained diabase dykes within plagiogranite. Roadcut west of Palaichori. Within the plagiogranite, elongated mafic minerals form a cardhouse structure within which the plagioclase crystallised later on, named cumulate fabric. [Stop GP33; ED3.1 is several hundred meters further to the NE]



Dark diabase dykes within plagiogranite. Dykes that thin out downwards, e.g. right of the center, indicate horizontal movement of melt. Same location as above. [Stop GP33]



Dark diabase dyke in sharp contact with grey plagiogranite. Towards the contact the plagiogranite shows no change in grain size, whereas the diabase gets darker and finer. From this observation it is evident that the diabase is intrusive into the somewhat cooled plagiogranite. Same location as above. [Stop GP33]



Angular fragment of plagiogranite within diabase dykes. This may give an impression how sheeted dykes intrude one into another, filling nearly vertical cracks in the upper oceanic crust. Same location as above. [Stop GP33]



Grey plagiogranite with mafic xenoliths. Same location as above. [Stop GP33]



Within plagiogranite, several darker and finer xenoliths point to contact of the plagiogranite magma with more mafic rocks at higher depth during ascent through the oceanic crust. Their undulating to subrounded shape points to marginal melting of the xenoliths and beginning assimilation into the host rock. Detail from above photo. [Stop GP33]



Kumulate fabric of plagiogranite, with mafic cumulate crystals, formed earlier, and plagioclase, crystallised later within the card house structures as intercumulus material. The fact that even few cm thick could be filled by dykes of diabase demonstrates that the host rock must have had high temperatures, as otherwise the intruding magma would have cooled at the contact surface and would have solidified. [Stop GP33]



Basaltic hyaloclastites without clear bedding, in the center, are covered by pillow lavas, above center, and both are intruded by near-vertical basaltic dykes. On the cover of (EDWARDS, S., et al. 2010) this famous outcrop is depicted. Akaki River at Agia Koroni, southwest of Klirou. [Stop ED 3.10; FM_Akaki-River2019-1: river sand]



Not all pillow-like basalts are in fact pillow lavas. Here a basaltic sheet flow is inclined towards the left. Former columnar joints in combination with weathering produced pillow-like structures within the columns, see e.g. same diameter of brownish pillows within one column left of center. Mathiatis Mine between Mathiatis and Agia Varvara. [Stop ED3.15]



Here thin similarly-inclined columns indicate sheet flows, their former cooling surface was oriented perpendicular to the columns. Northern slope of Mathiatis Mine [Stop ED3.15]



These are real pillow lavas! Irregular boundaries between pillows cannot result from weathering. Southern slope along the road, ascending to the lake at Mathiatis open pit mine. [Stop ED3.15]



Wedge-shaped packages of deformed, slumped sediments, concordant at the base, overly slightly southwards dipping well-bedded cherts, limestones and marlstones. The slump indicates either formerly relatively steep slopes or earthquake activity of both. Northwestern end of Kouris Dam. [Stop ED7.10]



Even bedding indicates undisturbed stillwater sedimentation. Sequence is very similar to basal unit visible in the former picture. Southeastern end of Kouris Dam. [Stop ED7.10]



Pleistocene shallow-marine conglomeratic sandstones document a formerly higher sea level or uplift of this part of the island. Dark pebbles are well-rounded mafic clasts, matrix consists of carbonaceous sandstone. Larnaca Salt Lake, close to northeastern roundabout north of the airport. The arrow points to a 1 € coin for scale. [West of stop ED6.17]



Along the shoreline of this salt lake, a lagoon separated from the open Mediterranean Sea, pore waters evaporate and salts and carbonates are precipitated, forming beachrock. A high amount of nutrients is indicated by the algal mats that form a broad marginal band in aerial images. Towards the right, marine Pleistocene conglomerates crop out. Larnaca Salt Lake, same location as before.



Greek and Roman metallurgists produced copper from sulfidic ores on Cyprus. The remains of these activities are still present in the form of black slags. Ancient slag heap close to the entrance to Skouriotissa Mine. [Stop ED7.3; FM_31.07.2019-1b]



Example of the ancient slags, same location as before. Due to the hardness of the material, many slag heaps were exploited for road construction material. Meanwhile they are protected by law and should not be destroyed. [Stop ED7.3]



Ancient slag, same location as before. See the large bubbles with smooth surfaces. Despite the extraction of copper, the high density of the slag indicates that large quantities of metals must still be present. [FM_31.07.2019-1b: 2x2 cm part from visible slag]



Strongylós Mine south of Mathiatis. Dark spots are entrances to antique road heads that were discovered during mine operations in the 20th century. White spots mark the occurrence of salts. The original rocks are severely altered and hardly to determine. If this area would be protected against further mining, it could provide insights into the old mining and ore processing techniques, an important part of ancient cultural development.



The ore body is mainly below water level, subaerial parts are indicated by dark grey colors left of center. Kokkinopezoula Mine at Mitsero; view from the lower part of heap at eastern margin of the open pit. [Stop GPM3&ED7.4]



White precipitation close to water level of the lake in the abandoned open pit may be gypsum or salts. Dark colour of the water is extraordinary and spectacular. It probably results from anoxic conditions and sulfide precipitation at the lake bottom, even at shallow water depth. Kokkinopezoula Mine at Mitsero. [Stop GPM3&ED7.4]



Oxidation of sulfides is evident by ochre and red colours on the northern part of the upper mine slopes: Iron hat above sulfidic ores. Yellow colors point to limonite or goethite, maybe also to jarosite, reddish ones to hematite, here associated with red jasper. The outcrop close to the margin of the open cut is covered by mine heap in the background. Kokkinopezoula Mine. [Stop GPM3&ED7.4; FM_28.07.2019-1: Jasper and hematite]



On the northern, here left, side of the lake in the grey rocks basaltic pillow lavas and sheet flows can be observed. They are covered by tailings with ochre colours. Mathiatis Mine. [Stop ED3.15; FM_1.08.2019-2: pyrite-impregnated basalt]



On these tailings leaching of acid pore waters and precipitation of white and green salts clearly indicate acid mine drainage. Sparse vegetation certainly is a consequence of both low pH and soil erosion by surface runoff and gullies, combined with seasonal aridity. Here one can study the effects of former mining activities without human remediation efforts. Mathiatis Mine. [Stop ED3.15]



Road head of Kannoures Mine north of Mt. Olympus. In the 19th century, chromite ore was mined here. The dimension and structure of the tunnel indicates a former relatively small technical investment. [Stop GP10&ED2.3]



In the 16th century, the heart-like bastions and the courtines, planned by Venetian architects, had to protect the renaissance city of Nicosia against osmanian attacks, but without long success. Inclination of walls was calculated to resist best against canon fire. Today parts of the formerly water-filled graben around the fortifications are used as parks, parking places and football fields. For historical details see www.wikipedia.de. Constanza Bastion, Nicosia.



	<p>Several dammed lakes provide water for irrigation on the seasonally rain-laden southern slopes of Troodos Massif. At a former lake level close to the level of the spillower, floating tree branches and plastics were washed over the barrier and deposited on the concrete floor. Kouris Dam. [Stop ED7.10]</p>
	<p>Former trampoline jumping sheet at landfill site northeast of Kotsiatis. This facility has been closed, but at least until February 2019, see journal dates, there has been wild deposition of garbage. This was an awful sight and it reminds us to reduce garbage as far as possible! [Stop ED7.13]</p>

Fig. 5.13-2: Impressions of outcrops visited during the excursion in 2019, sorted according to their stratigraphic position in the Cyprus lithology from old to young or deep to shallow, respectively. Stops: ED = (EDWARDS, et al. 2010), GP = Troodos Geopark, GPM = Mine in GP. For locations see [fig. 5.13-1](#).

[Back](#)

5.13.2. Classification of magmatic rocks of Troodos Ophiolite

For magmatic or igneous rocks various diagrams for classification are based either on modal composition in vol.-% (GILLESPIE, M.R. & STYLES, M.T. 1997), (LE MAITRE, R.W., et al. 2002), on their normative composition in wt.-% (LE MAITRE, R.W., et al. 2002) - which is usually limited to volcanic rocks -, or on oxide or element ratios, see e.g. (WILSON, M. 1989). In this study, diagrams were plotted with Geochemical Data kit, GCDkit, see http://www.gcdkit.org/pub/GCDkit_Hruba_Skala.pdf.

A mantle or plutonic rock name is commonly based on modal composition, i.e. using a macro- or microscopically determined content of mineral phases in volume-% and plotting the composition of main minerals in a diagram with classification boundaries. For a distinction between ortho- and clinopyroxene a microscopical inspection is necessary in most cases. In addition, the rock fabric is also used for classification, for an overview see e.g. (WIMMENAUER, W. 1985). The fabric identification allows the attribution of a sample to a rock family: mantle and plutonic rocks have more time for crystallisation and thus are

holocrystalline, i.e. all material is present as well-observable crystals, in contrast to faster solidified, typically porphyric, volcanic rocks where larger phenocrystals may or may not occur within a fine-grained or glassy groundmass or matrix; a family of subvolcanic dykes like dolerites stands in between both fabrics, being holocrystalline but with smaller crystal size and frequently developed as a porphyric fabric.

A problem for thin-section quantification of modal mineral content arises both for coarse- and fine-grained magmatic rocks:

1. From the relatively small area of a thin-section, roughly 2x3 cm, the content of different minerals can be determined from point-counting, but its representativeness may be questionable.
2. In the presence of a foliation and/or lineation, thin-sections should be studied in 3 orthogonally oriented slabs, which will be rarely performed. In a sheared zone of the upper mantle or lowermost oceanic crust a preferred orientation of elongated minerals like pyroxene has been frequently observed, see e.g. (NICOLAS, A. 1995), p. 116.
3. In subvolcanic dykes or volcanic rocks with a finegrained or glassy groundmass only phenocrysts can be determined.

Provided that geochemical analyses were performed on crushed material of several kilogram sized samples a classification based on normative mineral content may be more suitable for these coarse-grained plutonic rocks, and this approach is applicable for volcanic rocks as well. Therefore, in this study a classification based on normative mineral content was performed using literature data. It is planned to collect samples of plutonic and mantle rocks for geochemical analyses during a future excursion to Cyprus, as few literature data for these rock groups are available.

In comparison to plutonic rocks, volcanic rocks have less time for crystallisation. Here a classification based on geochemical analyses can be used to calculate a so-called normative composition, most frequently the procedure of the CIPW-Norm developed by CROSS, IDDINGS, PIRSSON and WASHINGTON in 1902, see e.g. <https://de.wikipedia.org/wiki/CIPW-Norm>, (WIMMENAUER, W. 1985), or (LE MAITRE, R.W., et al. 2002), has been applied. From major oxide and some trace element contents normative minerals potentially occurring in a rock sample are calculated. Classification of volcanic rocks is either based on xy- or ternary plots of main oxides or trace elements or on ternary or bi-ternary plots of the content of three to four modal or normative rock-forming minerals or on traceelement ratios. A couple of diagrams is offered from GCDkit (JANOUSEK, V., et al. 2006), automatically proposing diagrams for which essential parameters are available in the analysed dataset.

In this study, CIPW norms were calculated for geochemical analyses of various publications of mantle, plutonic and volcanic rocks from Cyprus using an Excel spreadsheet provided by KURT HOLLOCHER, Geology Department, Union College, Schenectady, NY, 12308, hollochk@union.edu. Disadvantages of this approach are:

1. only water-free minerals like pyroxenes can be calculated, but no water-bearing amphiboles or micas.
2. only a limited number of minerals is calculated, e.g. only one ortho- and two clinopyroxenes.
3. the severe impact of the molar $\text{Fe}^{3+}/\text{Fe}_{\text{tot}}$ or $\text{Fe}_2\text{O}_3/\text{FeO}$ ratio (MIDDLEMOST, E.A.K. 1989) is crucial for the calculation of Fe-bearing normative minerals: magnetite, ilmenite, hematite, chromite, olivine, hypersthene, diopside, aegirine, pyrite; unfortunatley, few publications list both FeO and Fe_2O_3 contents from e.g. photometric quantification. At least for these individual samples the $\text{Fe}^{3+}/\text{Fe}_{\text{tot}}$ ratio

has to be estimated, an alternative is the assumption of a fix molar ratio for all samples of a specific rock type, an approach applied in this study.

In the following selected plots show classifications of magmatic rock types from Cyprus based on:

1. CIPW norms calculated from chemical whole rock analyses in volume-%, for better comparability with modal content, and not in weight-% as was suggested by (LE MAITRE, R.W., et al. 2002), p. 4, only for volcanic rocks;
2. primary geochemical data, taken from literature, plotted in specific diagrams.

At first, normative compositions of ultramafic rocks of Troodos Massif with a content of mafic minerals ≥ 90 vol.-%. will be discussed. As ternary diagram that of [fig. 5.13-3](#), see (STRECKEISEN, A. 1973), was chosen, considering normative olivine $(\text{Fe}^{2+}_{0.1}\text{Mg}_{0.9})_2\text{SiO}_4$, hypersthene, $(\text{Fe}^{2+}_{0.3-0.6}\text{Mg}_{0.3-0.6})_2\text{Si}_2\text{O}_6$, as orthopyroxene and diopside, $\text{CaMgSi}_2\text{O}_6$, as clinopyroxene. Mineral formula in this study are taken from (DYAR, M.D., et al. o.a.), sometimes completed with indices given in (NICOLAS, A. 1995) or (TRÖGER, W.E., et al. 1982).

Table 5-13.2: Compilation on literature providing geochemical analyses for lithostratigraphical units. Entries retrieved from the GEOROC database are marked by *. N = number of analyses. References are given if ≥ 5 individual analyses were published in a paper, but excluding papers that presented exclusively averaged analytical data. Here are listed all analyses available to the best of our knowledge including those where no major elements were presented. Newer articles do no longer differentiate between separate units within the Volcanic Series. The color coding of this table is also applied in most of the following plots of geochemical data.

Lithostatigraphical unit	Reference	N
Kannaviou Form., Sed.	(CHEN, G. 2018)	20
Perapedhi Form., Sed.	(ROBERTSON, A.H.F. 1973), (ROBERTSON, A.H.F. 1978)	9
Perapedhi Form./UPL, ochre	(ROBERTSON, A.H.F. & FLEET, A.J. 1976)	3
Perapedhi Form., umber	(RAVIZZA, G., et al. 1999)	8
	(ELDERFIELD, H., et al. 1972)	6
	(PRICHARD, H.M. & MALIOTIS, G. 1998)	16
	(ROBERTSON, A.H.F. 1973), (ROBERTSON, A.H.F. 1978)	19
Volcanic Series, undiff.	(BAILEY, D.G. 1984)	24
	(BEDNARZ, U. & SCHMINCKE, H.-U. 1994)	19
	(COOGAN, L.A. & GILLIS, K.M. 2018)*, (PATTEN, C.G.C., et al. 2017)	270
	(KOSTOPOULOS, D.K. & MURTON, B.J. 1992), (GOLOWIN, R., et al. 2017)	13
	(KURZWEIL, F., et al. 2019)	5
	(PORTNYAGIN, M.V., et al. 2002)	13
	(THY, P., et al. 1985)	12
(WÖLKI, D., REGELOUS, M., et al. 2019)	374	
Volcanic Series, Upper Pillow Lavas, basalt, basaltic andesite	(BAILEY, D.G. 1984), (BAILEY, D.G., et al. 1991)	68
	(CAMERON, W.E. 1985)	28
	(COOGAN, L.A. & GILLIS, K.M. 2018)*	48
	(FLOWER, M.F.J. & LEVINE, H.M. 1987)	30
	(FONSECA, R.O., et al. 2017)	23
	(GILLIS, K.M., et al. 2015), (BRANT, C.O. 2014)	93
(OHNENSTETTER, M., et al. 1990)	11	

	(OSOZAWA, S., et al. 2012)	10
	(PEARCE, J.A. & ROBINSON, P.T. 2010)	27
	(TAYLOR, R.N. 1990)	5
Volcanic Massif Sulfides	(CONSTANTINOU, G. & GOVETT, G.J.S. 1973)	33
	(HANNINGTON, M.D., et al. 1990)	6
Volcanic Series, Lower Pillow Lavas, boninite, tholeiite, basaltic andesite, andesite	(BAILEY, D.G. 1984)	8
	(COOGAN, L.A. & GILLIS, K.M. 2018)	61
	(FLOWER, M.F.J. & LEVINE, H.M. 1987)	18
	(GILLIS, K.M., et al. 2015), (BRANT, C.O. 2014)	58
	(OSOZAWA, S., et al. 2012)	9
	(PATTEN, C.G.C., et al. 2017)	18
	(PEARCE, J.A. 1975), (PEARCE, J.A. & ROBINSON, P.T. 2010)	46
	(PORTNYAGIN, M.V., et al. 1997)	11
	(RAUTENSCHLEIN, M., et al. 1985)	7
Volcanic Series, Basal Group	(REGELOUS, M., et al. 2014)	80
	(FLOWER, M.F.J. & LEVINE, H.M. 1987)	9
	(PATTEN, C.G.C., et al. 2017)	5
	(PEARCE, J.A. & ROBINSON, P.T. 2010)	70
Sheeted Dyke Sequence, Diabase	(ASH, C.H. 1990)	17
	(BANKS, G.J. 2004), (BARAGAR, W.R.A., et al. 1990)	25
	(GILLIS, K.M. & COOGAN, L.A. 2002)	26
	(JOWITT, S.M., et al. 2012)	137
	(PEARCE, J.A. 1975)	13
	(RICHARDSON, C.J., et al. 1987)	8
Mafic dykes within Plutonic Series	(BANKS, G.J. 2004)	5
	(COOGAN, L.A. 2003)	6
Plutonic Series, Plagiogranite, Tonalite, Trondhjemite	(FREUND, S., et al. 2014)	24
	(MARIEN, C.S., et al. 2019)	21
	(PATTEN, C.G.C., et al. 2017)	6
Plutonic Series, qtz-Gabbro	(MARIEN, C.S., et al. 2019)	6
Plutonic Series, Gabbro, Gabbro-norite	(ASH, C.H. 1990)	11
	(BANKS, G.J. 2004)	53
	(CHUM, C.-Y. 2014)	7
	(PATTEN, C.G.C., et al. 2017)	11
	(PRICHARD, H.M. & LORD, R.A. 1990)	21
Plutonic Series, Pyroxenite, Websterite, Gabbro-norite	(ASH, C.H. 1990)	29
	(BANKS, G.J. 2004)	25
	(BÜCHL, A., BRÜGMANN, G.E., et al. 2004)	5
	(CHUM, C.-Y. 2014)	25
Plutonic Series, Wehrlite	(ASH, C.H. 1990)	31
	(CHUM, C.-Y. 2014)	5
	(PRICHARD, H.M. & LORD, R.A. 1990)	14
Mantle Sequence, Chromitite	(GREENBAUM, D. 1977)	5
Mantle Sequence, Dunite	(ASH, C.H. 1990)	16
	(BÜCHL, A., et al. 2002), (BÜCHL, A., BRÜGMANN, G.E., et al. 2004)	18
	(BÜCHL, A., et al. 2002)*, (BÜCHL, A., BRÜGMANN, G.E., et al. 2004)	15

From the following ultramafic rock types lherzolite, dunite, harzburgite and chromitite are considered as mantle rocks, pyroxenite and wehrlite as plutonic rocks. References for the analyses are given in [table 5.13-2](#). For classification and reclassification, respectively, the diagram in [fig. 5.13-3](#) was used. This certainly does not mean that the reclassification based

on normative mineral content presented in the following is more accurate than that given in the original publication, but this procedure has the advantage that all available analyses are handled in the same manner, which is essential for calculation of median values for different rock types. Another diagram using pyroxene, olivine and hornblende, see (LE MAITRE, R.W., et al. 2002), p. 28, cannot be applied when plotting normative mineral content, as CIPW norm does not calculate hornblende.

- For 5 lherzolite samples from Troodos Massif the median of molar $\text{Fe}^{3+}/\text{Fe}_{\text{tot}}$ ratios of 37 samples from worldwide locations in the GEOROC database, <http://georoc.mpch-mainz.gwdg.de/georoc/>, retrieved in June and July 2021, excluding xenoliths, of 0.2842 was used in this study. This value may be somewhat too high, as some of the samples plot in the harzburgite field. Using a value of 0.1261 as for dunite, see below, would tendentially improve the fit into the plot field for lherzolite, but not substantially. One sample: TV-220/1 from (BÜCHL, A., BRÜGMANN, G.E., et al. 2004), was reclassified as harzburgite, another: CA-T37.4 from (ASH, C.H. 1990), as olivine-websterite. Together with reclassified samples attributed to other ultramafics in the original papers there are now in total 23 lherzolite rock analyses available.
- For 30 dunite samples from Troodos Massif the ratio $\text{Fe}^{3+}/\text{Fe}_{\text{tot}}$ also had to be taken from a median calculated from 58 analyses of worldwide dunite samples in GEOROC, again excluding xenoliths, providing a value of 0.1261. Most samples plot in the dunite field. However, 3 samples were reclassified as harzburgite: T4cb, T4d (BÜCHL, A., BRÜGMANN, G., et al. 2004), CA-T2 (ASH, C.H. 1990), one as lherzolite: T10 (PATTEN, C.G.C., et al. 2017), one as olivine-websterite: CA-T26 (ASH, C.H. 1990); remaining 26 dunite samples, including reclassified samples of other rock types.
- For 18 harzburgite samples from Troodos Massif, a median ratio $\text{Fe}^{3+}/\text{Fe}_{\text{tot}}$ of 0.0701 from 276 samples in GEOROC, excluding xenoliths, had to be applied. All of the samples besides one plot in the harzburgite field. The latter sample, TV98-15 (BÜCHL, A., BRÜGMANN, G.E., et al. 2004), was reclassified as dunite. Low normative magnetite, Fe_3O_4 , content of 0.6 vol.-% correlates with low measured magnetic susceptibility, see [table 5.13-2](#). Together with reclassified samples a total of 25 harzburgite samples remains.
- For 5 chromitite samples from Troodos Massif a median ratio $\text{Fe}^{3+}/\text{Fe}_{\text{tot}}$ of 0.1635 can be calculated from published analyses, which is in contrast to the higher value of 0.5645 for only 2 values available in GEOROC. For ratios ≤ 1 as well as for measured ratios, i.e. using FeO and Fe_2O_3 in the original measured ratio for all samples, no normative magnetite results. This coincides with – compared to other rock types – low magnetic susceptibility, but there must exist at least some magnetite, see [table 5.13-2](#). These rocks cannot be classified according to [fig. 5.13-3](#) as they represent SiO_2 -poor ores.
- Wehrlite is an ultramafic rock consisting almost exclusively of clinopyroxene and olivine. 30 wehrlite analyses from Troodos Massif were taken from (ASH, C.H. 1990) and as $\text{Fe}^{3+}/\text{Fe}_{\text{tot}}$ ratio a value of 0.2948, a median calculated from only 12 analyses of wehrlite in GEOROC from worldwide places, was used as a starting point. The samples would not plot within the wehrlite field but in the harzburgite, lherzolite and olivine-websterite fields. If a lower $\text{Fe}^{3+}/\text{Fe}_{\text{tot}}$ ratio of 0.2, 0.1 or 0.05 is applied, points move towards but with one exception do not yet enter the wehrlite field. After comparison with ratios assumed for the other ultramafic rocks, a value of 0.1 seems more reasonable. Surprisingly, (ASH, C.H. 1990), p. 39, mentioned: „Orthopyroxene is a common accessory phase throughout the unit and rarely increases to 10 or 20 modal percent where it occurs as large (1 -1.5 cm) oikocrysts poikilitically enclosing

both olivine and clinopyroxene.“ If we take into account that for plotting samples in the diagram of [fig. 5.13-3](#) only three major components of the modal composition are summarized as 100 vol.-%, their absolute abundances in a rock sample should be even lower. BUT: applying the classification scheme in [fig. 5.13-3](#), only samples with ≤ 5 modal % of orthopyroxene in the total of $opx+cpx+ol$ may be classified as wehrlite! Four samples: CA-T30, CA-T37.1, CA-T47, CA-T60, contain more than 10 vol.-% normative felsic minerals and should be reclassified as gabbros (?). Three samples: CA-T28.4, CA-T35, CA-T37.2, contain less than 40 vol.-% normative olivine and were reclassified as olivine-websterite. Four samples that contain less than 5 vol.-% normative diopside were reclassified as harzburgite: CA-T8, CA-T10, CA-T38, CA-T48.2. All remaining samples: CA-T9, CA-T24, CA-T28.3, CA-T31, CA-T39, CA-T44, CA-T45, CA-T48.1, CA-T48.3, CA-T48.4, CA-T48.6, CA-T49, CA-T54, CA-T55, CA-T56, CA-T57, CA-T59, CA-T62, CA-T63 plot within the lherzolite field and were correspondingly reclassified. From further 14 samples of (PRICHARD, H.M. & LORD, R.A. 1990) and (CHUM, C.-Y. 2014) no major element oxides are available. Thus it follows that so far no wehrlite samples are available from the literature data under consideration!

- 56 samples were classified in the original publications as pyroxenite, ortho-pyroxenite, clino-pyroxenite, websterite, olivine-websterite, sometimes in combination of several names and partly in combination with gabbro; based on the data treatment proposed in this study with exception of the latter these rock types correspond to pyroxenite s.l. or sensu (LE MAITRE, R.W., et al. 2002), respectively. In data given in the GEOROC database the median Fe^{3+}/Fe_{tot} ratio of 855 pyroxenite samples of the world is 0.0835, excluding xenolithic samples, which was as well assumed for the Troodos Massif samples as a plausible value. With the exception of only two analyses: CA-T32.1 and CA-T32.2 (ASH, C.H. 1990), all 54 samples plot in the fields below 40 vol.-% olivine, i.e. in the domain of pyroxenite s.l., the two analyses mentioned were reclassified as gabbro (?) as they contain more than 60 % felsic minerals.

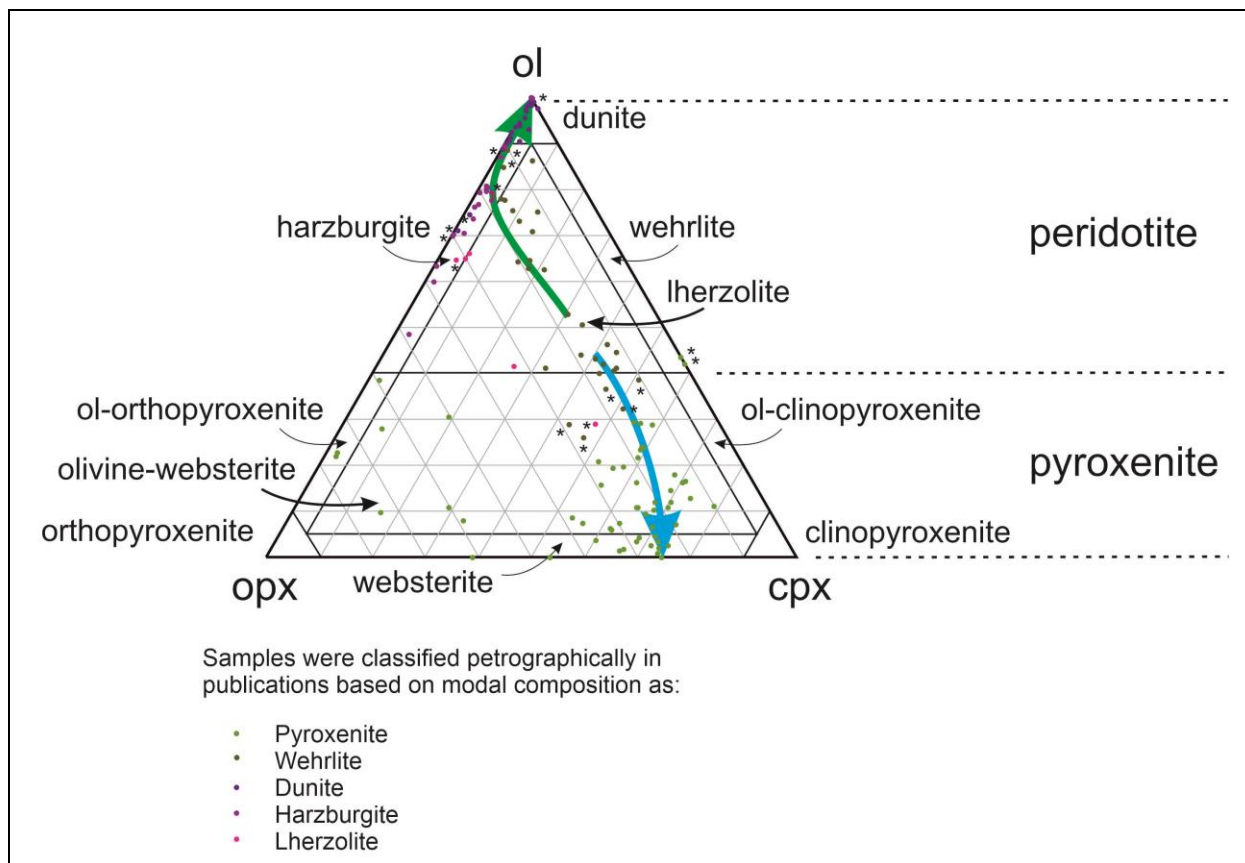


Fig. 5.13-3: Normative mineral content of ultramafic rocks from Troodos Massif calculated using the CIPW norm spreadsheet from KURT HOLLOCHER in volume-% for literature data, see [table 5.13-2](#), plotted in a diagram for the classification of ultramafic rocks developed by (STRECKEISEN, A. 1973). Abbreviations: ol = olivine, opx = orthopyroxene, cpx = clinopyroxene. Rocks with > 40 and < 90 vol.-% olivine are grouped as pyroxene peridotite sensu (GILLESPIE, M.R. & STYLES, M.T. 1997) or peridotite sensu (LE MAITRE, R.W., et al. 2002), those with < 40 and > 10 vol.-% as olivine pyroxenite sensu (GILLESPIE, M.R. & STYLES, M.T. 1997) or pyroxenite sensu (LE MAITRE, R.W., et al. 2002) and those with < 10 vol.-% as pyroxenite s.s.. An * marks samples that were reclassified in this study, for the group of wehrlite samples plotting within the lherzolite field this symbol was omitted for clarity of the figure. Most samples have a moderate normative opx content of 10-30 vol.-%, which might represent the content in the parental mantle. The green arrow indicates depletion of the upper mantle in cpx by partial melting, leading to residual harzburgite and finally dunite; the blue arrow indicates enrichment of cpx in partial melts, both curves starting at a hypothetical parental lherzolite composition. The arrows are hypothetical, just for visualisation how these processes, described e.g. in (NICOLAS, A. 1995), could change mantle composition, arrows are not based on any other data or models.

In the ophiolite crust above the ultramafic rocks predominantly mafic plutonic rocks form an intermediate layer. Gabbroic rocks predominate with - from bottom to top - layered gabbro, isotropic gabbro with quartz-gabbro intrusions and uppermost patches of plagiogranite intrusions (EDWARDS, S., et al. 2010). Also from STRECKEISEN a ternary diagram for the classification of mafic rocks with < 90 vol.-% mafic minerals was developed using pyroxene, plagioclase and olivine (LE MAITRE, R.W., et al. 2002), p. 25, see [fig. 5.13-4](#). Apart from samples mainly consisting of only one of the three minerals, an additional ternary diagram plotting orthopyroxene, plagioclase and clinopyroxene contents can be used for further classification of gabbroic samples. Three principal rock groups of gabbroic rocks can then be distinguished: gabbro with clinopyroxene, norite with orthopyroxene and gabbronorite

containing both pyroxenes at about equal quantities. Again, a diagram using pyroxene, plagioclase and hornblende cannot be used for normative mineral contents. In the famous bi-ternary QAPF diagram of STRECKEISEN depicting Q = quartz, A = alkalifeldspar, P = plagioclase, F = foids (LE MAITRE, R.W., et al. 2002), p.22, gabbros and diorite contain < 5 vol.-% of quartz and less than ca. 10 vol.-% of alkalifeldspar as well as < 10 vol.-% foids. The distinction between gabbro and diorite is made at a limit of 50 vol.-% of anorthite content in plagioclase, with lower content in diorite and higher content in gabbro (LE MAITRE, R.W., et al. 2002), p. 24. If in the QAPF diagram between 5 and 20 vol.-% of quartz are present then the prefix quartz- is added, resulting in quartz-gabbro, quartz-diorite and quartz-anorthosite.

- 79 samples from Troodos Massif were described as gabbroic in the original publications: gabbro, olivine-gabbro or gabbro. From only 3 samples a mean Fe^{3+}/Fe_{tot} ratio of 0.2241 can be calculated, which would be 0.1 higher than that supposed for the mantle rocks, see above, which seems not implausible. For 907 worldwide samples of gabbro in GEOROC a median Fe^{3+}/Fe_{tot} ratio of 0.2976 resulted, however based on samples originating from varying plate tectonic situations. Here the ratio of 0.2241 was applied for norm calculations. 3 samples: AM-1G (FLOWER, M.F.J. & LEVINE, H.M. 1987), KG9945 (GILLIS, K.M. & COOGAN, L.A. 2002), CG10-CY3 (GRIMES, C., et al. 2013) contain > 5 vol.-% normative quartz and thus were reclassified as quartz-gabbro. The normative foid nepheline occurs in only 4 samples: CA-T21, CA-T32.4, CA-T32.1, CA-T32.2 (ASH, C.H. 1990), the latter two originally classified as wehrlite. Thus, in the QAPF diagram most gabbros from Troodos Massif would plot in the upper, silica-saturated, part.
- For 6 quartz-gabbros and further 3 reclassified samples, see above, a mean Fe^{3+}/Fe_{tot} ratio of 0.3 may be supposed. Unfortunately, this rock-type is not listed in GEOROC. One of the 6 samples had to be reclassified as plagiogranite as it contains >20 vol.-% normative quartz: Cy 86b (MARIEN, C.S., et al. 2019).
- 62 samples were originally classified as plagiogranite or trondhjemite or as plagiogranite/diorite or plagiogranite/tonalite. The sample amount in relation to the portion that these rocks take within the plutonic series demonstrates the higher interest in this evolved rock type compared to common gabbroic rocks. In the QAPF diagram light-coloured plagiogranites and trondhjemites plot in the field of tonalites limited by 20 to 60 vol.-% quartz and more than ca. 90 vol.-% of plagioclase, remaining less than ca. 10 vol.-% kalifeldspar. This results in a low K-content of the material, with a median of 0.19 wt.-% K_2O . From 5 samples from Troodos Massif a median Fe^{3+}/Fe_{tot} ratio of 0.5750 resulted. For 136 worldwide tonalite samples in GEOROC a median ratio of 0.3757 can be calculated. As a starting point, the value of 0.5750 was used for norm calculations. Two samples, TroSpi 31 and TroSpi33 (FREUND, S., et al. 2014), were reclassified as quartz-rich granitoid, see [fig. 5.13-5](#). But: the high magnetic susceptibility, see [table 5.13-2](#), suggests that the ratio might be somewhat too high.

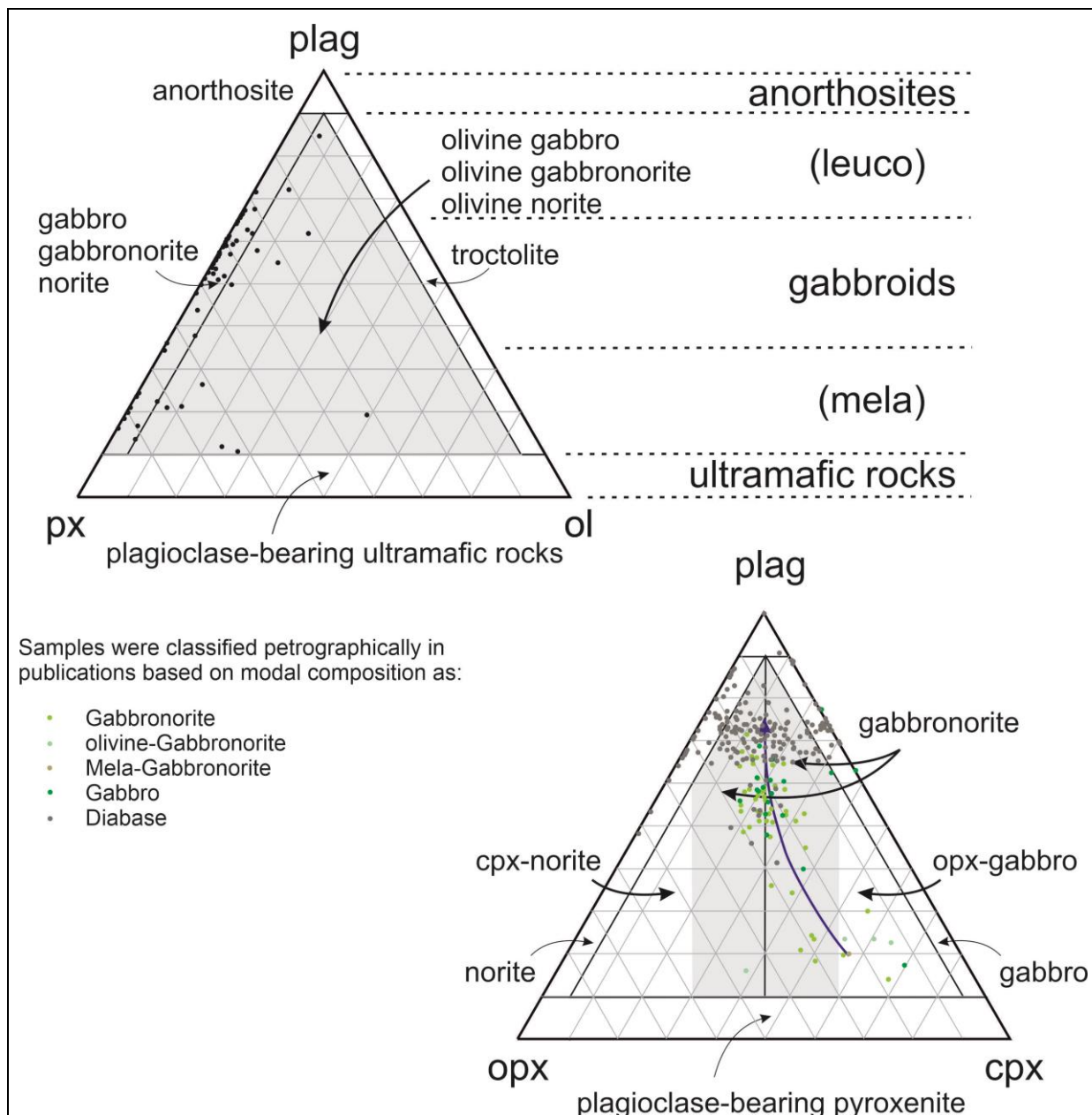


Fig. 5.13-4: Gabbroic sample classification in diagrams developed by STRECKEISEN, see (LE MAITRE, R.W., et al. 2002) using the CIPW norm spreadsheet from KURT HOLLOCHER in volume-% for literature data, see [table 5.13-2](#). For samples in the grey shaded area in the upper left diagram a further classification using the lower right diagram is possible (LE MAITRE, R.W., et al. 2002), which is applicable for all samples. Gabbronorite is a rock consisting of opx and cpx in a similar content - together with plag -, see the approximate area indicated by a grey shading in the lower right diagram. As is the case with ultramafic rocks in [fig. 5.13-3](#), the content of orthopyroxene is between 10 and 30 vol.-% for most samples. Diabase samples are added in the lower right diagram, as their petrographical classification should be microgabbro. The blue arrow marks a possible trend for melt composition changing from gabbroic towards tonalitic composition through fractional crystallisation, comprising enrichment of cpx and plagioclase together with depletion of opx, within melts rising from the liegend plutonic level to that of the hanging Sheeted Dyke Series. The arrow is again not based on further data.

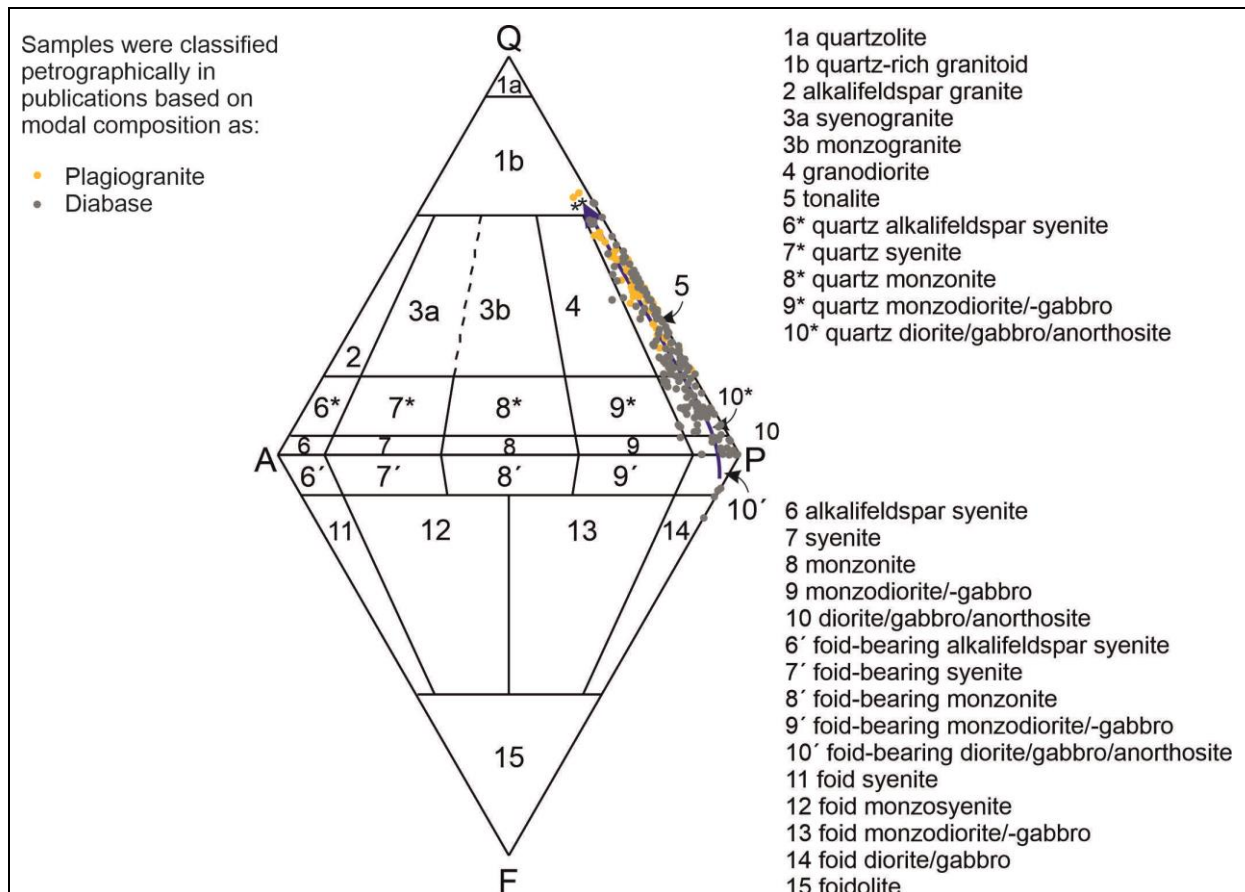


Fig. 5.13-5: Plagiogranite and diabase samples of literature data, see [table 5.13-2](#), plotted in the QAPF diagram for plutonic rocks, using the CIPW norm spreadsheet from KURT HOLLOCHER in volume-%. Two samples, marked with an asteriks, were reclassified as quartz-rich granitoids. The blue arrow indicates the probable evolution of gabbroic to granitoid composition of the melt during fractional crystallisation, again this is not based on further data but shows a visualisation of possible melt development.

Above the plutonic rocks there exists a subvolcanic Sheeted Dyke Complex which petrographically consists of diabase. Diabase formerly was used for altered basalt or basalt with a so-called, ophitic fabric (LE MAITRE, R.W., et al. 2002). In modern classification microgabbro is used as a synonym for diabase or dolerite (LE MAITRE, R.W., et al. 2002). These rocks have a holocrystalline fabric similar to that of gabbros but with smaller crystal size due to more rapid cooling. The hydrothermal alteration of diabase in Troodos Massif is more intense compared to rocks of the Plutonic Series, evident from the occurrence of green minerals like epidote, $\text{Ca}_2(\text{Fe}^{3+}, \text{Al})_3(\text{SiO}_4)(\text{Si}_2\text{O}_7)(\text{OH})$, similar in composition to a hydrated clinopyroxene, and chlorite, $\text{Mg}_3\text{Mg}_2\text{Al}(\text{Si}_3\text{Al})\text{O}_{10}(\text{OH})_8$, a mica-like phyllosilicate that often replaces biotite, see e.g. (EDWARDS, S., et al. 2010).

- Rocks of the Sheeted Dyke Complex in Troodos Massif stand in between the liegend plutonic and hanging volcanic rock series. In the original papers rock samples of the Sheeted Dyke Complex or Series were classified as diabase, sometimes with indication of basaltic or andesitic composition; sometimes classified as diabase-epidosite, epidosite, a chlorite-quartz-epidote rock, but not a common magmatic rock name; a group of 10 dyke samples were classified as basalt, andesite, Mid-Oceanic Ridge Basalts or MORB-like dykes, Island-Arc-Tholeiites or IAT-like dykes, boninitic dykes; the latter group is not further discussed in this manuscript but data were plotted together with the other analyses in several of the following diagrams. The median $\text{Fe}^{3+}/\text{Fe}_{\text{tot}}$ ratio of 8 samples is 0.3992, which was used in this study. In

GEOROC a median ratio of 0.2340 can be calculated from 744 worldwide samples, but as stated above, some of these so-called diabase rocks may be altered basalts and the samples come from different plate tectonic settings. 5 of 229 samples from Troodos Massif are Si-undersaturated and plot in the foid-bearing gabbro and foid gabbro fields of the QAPF diagram, see [fig. 5.13-5](#). Most samples of the Sheeted Dyke Series plot in the quartz gabbro and tonalite field, some plot in the gabbro field. Concerning normative mineral composition, most of the diabase rocks from Troodos Massif cannot be classified as microgabbros. Together with [fig. 5.13-4](#) this points to either

- an enrichment of Si by fractionated crystallisation,
- a pneumatolytical to hydrothermal alteration during and after solidification supplied Si leached from other rocks,
- or a lot of dykes did not feed the predominantly basaltic pillow lavas and hyaloclastics solidified at or close to the seafloor, but supplied the melt for the hanging lower part of the Volcanic Series, the Basal Group of the former classification. These rocks are relatively similar in normative mineral composition, see [fig. 5.13-6](#).

As stated already in the caption of [table 5.13-1](#), a former subdivision of the Volcanic Series in a Basal Group, Lower Pillow Lava Series, Volcanic Massif Sulfides, VMS, and Upper Pillow Lava Series has been replaced by a slightly different nomenclature. An argument for the former stratigraphy was the distribution of mapped geological units. Meanwhile many samples are just ranked as Volcanic Series without further subdivision. This has the disadvantage that the internal vertical layering is no more represented in the denomination. In the following, first an overview on samples arranged in the older stratigraphy is shown, followed by samples in the Volcanic Series undifferentiated. Some samples are classified after their fabric, e.g. as lava, pillow, sheet, breccia, dyke, without geochemical characterization, not further mentioned in the following but plotted together with the other samples in [fig. 5.13-6](#). Many samples are still glassy, without alteration (WÖLKI, D., et al. 2018), which is quite extraordinary for Upper Cretaceous volcanic rocks. The latter peculiarity might explain the high amount of 1742 analysed samples, compared to 302 analyses of Sheeted Dyke Series, 304 analyses of Plutonic Series and 97 mantle rock analyses retrieved from literature in this study.

- In the Basal Group, samples were classified – listed approximately in the sequence of increasing SiO₂ - as Tholeiite, basaltic andesite, andesite, dacite, rhyodacite, which covers compositions resulting from quite distinct degrees of fractional crystallisation. Only one reported Fe³⁺/Fe_{tot} ratio is 0.1805, which was not used here and this is valid for all rocks reported from the Volcanic Series, see below. In the QAPF diagram, see [fig. 5.13-6](#), normative compositions of 83 analyses plot in the right part of the dacite field and in the gabbro/andesite field, very similar to the distribution of diabase samples in [fig. 5.13-5](#).
- In the Lower Pillow Lava Series 227 samples were classified as picrite, Boninite, basalt, Tholeiite, basaltic andesite. From 8 samples a median Fe³⁺/Fe_{tot} ratio of 0.1633 can be calculated. The variability of compositions in [fig. 5.13-6](#) is larger compared to the Basal Group samples, which partly may be due to the larger amount of analyses. The majority of samples plots in the basalt/andesite and dacite field. As median anorthite-content of plagioclase is ca. 61 vol.-%, more samples will be of basaltic than of andesitic composition. The high content of quartz in some samples, see upper end of yellow arrow, points to hydrothermal supply of silica. The pink arrow indicates magmatic differentiation and/or supply of potassium by hydrothermal solutions

originating either from leaching of other rocks or advected from sea water percolating through joints in the oceanic crust.

- For rocks of the VMS no major element contents are given.
- In the Upper Pillow Lava Series samples were classified as komatiite, picrite, olivine basalt, basalt, Tholeiite, basaltic andesite, andesite. A median Fe^{3+}/Fe_{tot} ratio of 0.2693 can be calculated from 51 analyses. 366 samples plot in [fig. 5.13-6](#) in the fields mentioned above for the Lower Pillow Lava Series plus further fields, with a larger group of samples in the quartz latite, latite and foid-bearing latite field. There are some more samples in the lower half of the QAPF diagram, but this may again result from the higher sample amount.
- In newer articles the composition of glassy Volcanic Series rocks was attributed to Boninite, basalt, Tholeiite, in pre 2000 articles of (BAILEY, D.G. 1984), (BEDNARZ, U. & SCHMINCKE, H.-U. 1994), (KOSTOPOULOS, D.K. & MURTON, B.J. 1992), (PORTNYAGIN, M.V., et al. 2002), (THY, P., et al. 1985) without stratigraphic differentiation as basaltic andesite to rhyolite. The median Fe^{3+}/Fe_{tot} ratio of only 20 analyses is 0.2598. From figures with sampling sites it can be assumed that most of the samples analysed would stratigraphically correspond to the Upper Pillow Lava Series, see e.g. (COOGAN, L.A., et al. 2017), (WÖLKI, D., P., M., et al. 2019), which is supported by the similar Fe^{3+}/Fe_{tot} ratios. In [fig. 5.13-6](#) 876 samples plot in the same fields as the Upper Pillow Lava Series samples, with some more samples in the trachyte field. This indicates magmatic differentiation in shallow magma chambers with late crystallisation of kalifeldspar, probably connected to plagiogranite intrusions.
- As a compromise, the Fe^{3+}/Fe_{tot} ratio for Basal Group and Lower Pillow Lavas is assumed here to be 0.17, and that of the Upper Pillow Lavas and Volcanic Series undifferentiated as 0.26, used for the data plotted in [fig. 5.13-6](#).

It must be stated here that modern publications do not show the QAPF diagram but xy- or ternary plots of major and trace element content or element ratios. One reason is that alkalis that take substantial positions in the feldspar lattice are much more mobile during alteration processes resulting in feldspar metasomatism compared to other major elements like e.g. Ti, trace elements like Zr, or Rare Earth Elements, REE, see e.g. (SALMINEN, R. 2005). In the following figures, some oxide and element contents and ratios, respectively, are plotted for classification of the volcanic rocks.

In [fig. 5.13-7](#) the total alkali-silica, or TAS, diagram of (COX, K.G., et al. 1979), similar - but with different field margins - to a diagram developed by (LE BAS, M.J., et al. 1986), is shown. It is evident that within this diagram there is enormous scatter of the samples, without any distinct trend due to magmatic differentiation. This is certainly a consequence of mobility of alkalis and silica during hydrothermal alteration.

In [fig. 5.13-8](#) more major elements are used for the classification after (ROCHE, H.D.L. & LETERRIER, J. 1980): Si, Fe, Ti, Na, K, Al, Mg, Ca. Again the high mobility of alkalis is certainly the reason for the wide scattering of the samples. Similar to [fig. 5.13-7](#), there are both low and high differentiated rocks, but again without a clear trend.

In [fig. 5.13-9](#) a diagram published by (WINCHESTER, J.A. & FLOYD, P.A. 1976), plotting the incompatible element ratio Nb/Y versus Zr/TiO_2 , is used for analyses of the volcanic rocks of Troodos Massif. Most samples plot within a trend from subalkaline basalt towards andesite/basalt, few samples are located in the andesite field. The lack of samples that would plot in the fields of differentiated volcanics like rhyodacite, dacite, trachyte, in contrast to the sample scatter in diagrams of [figs. 5.13-7](#) and [-8](#), is an argument for alkali mobilisation during hydrothermal circulation in the oceanic crust.

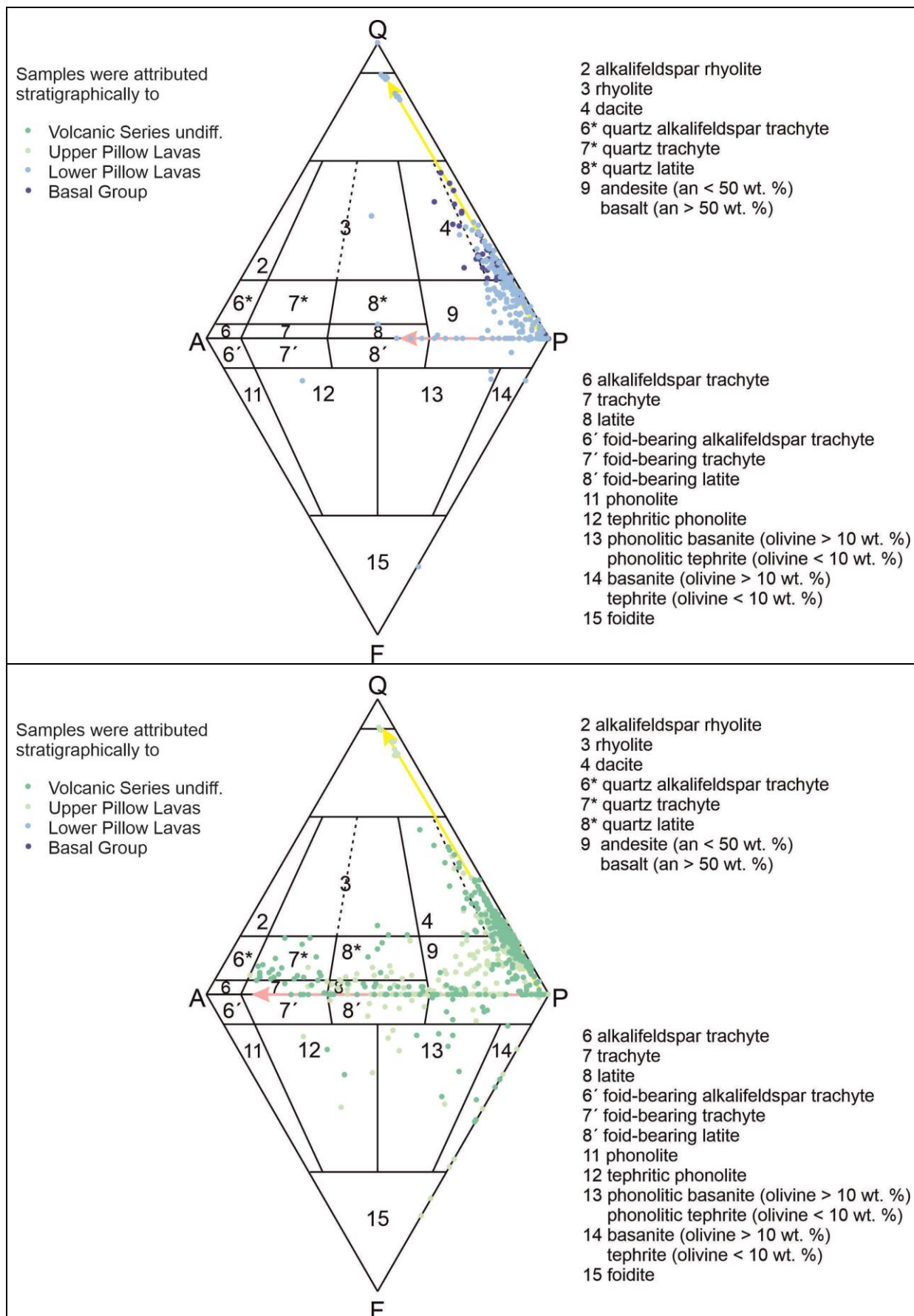


Fig. 5.13-6: QAPF diagram after Streckeisen for volcanic rocks of the Basal Group and the Lower Pillow Lava Series, upper part, and of the Upper Pillow Lava Series and Volcanic Series undifferentiated – but predominantly from an equivalent part of the crust -, lower part,

from Troodos Massif. The yellow arrow marks increasing Quartz content, at least in the uppermost part of the diagram indicative for supply of additional silica from hydrothermal solutions, and the pink arrow shows an increase of potassium content due to fractionated crystallisation and/or hydrothermal alteration.

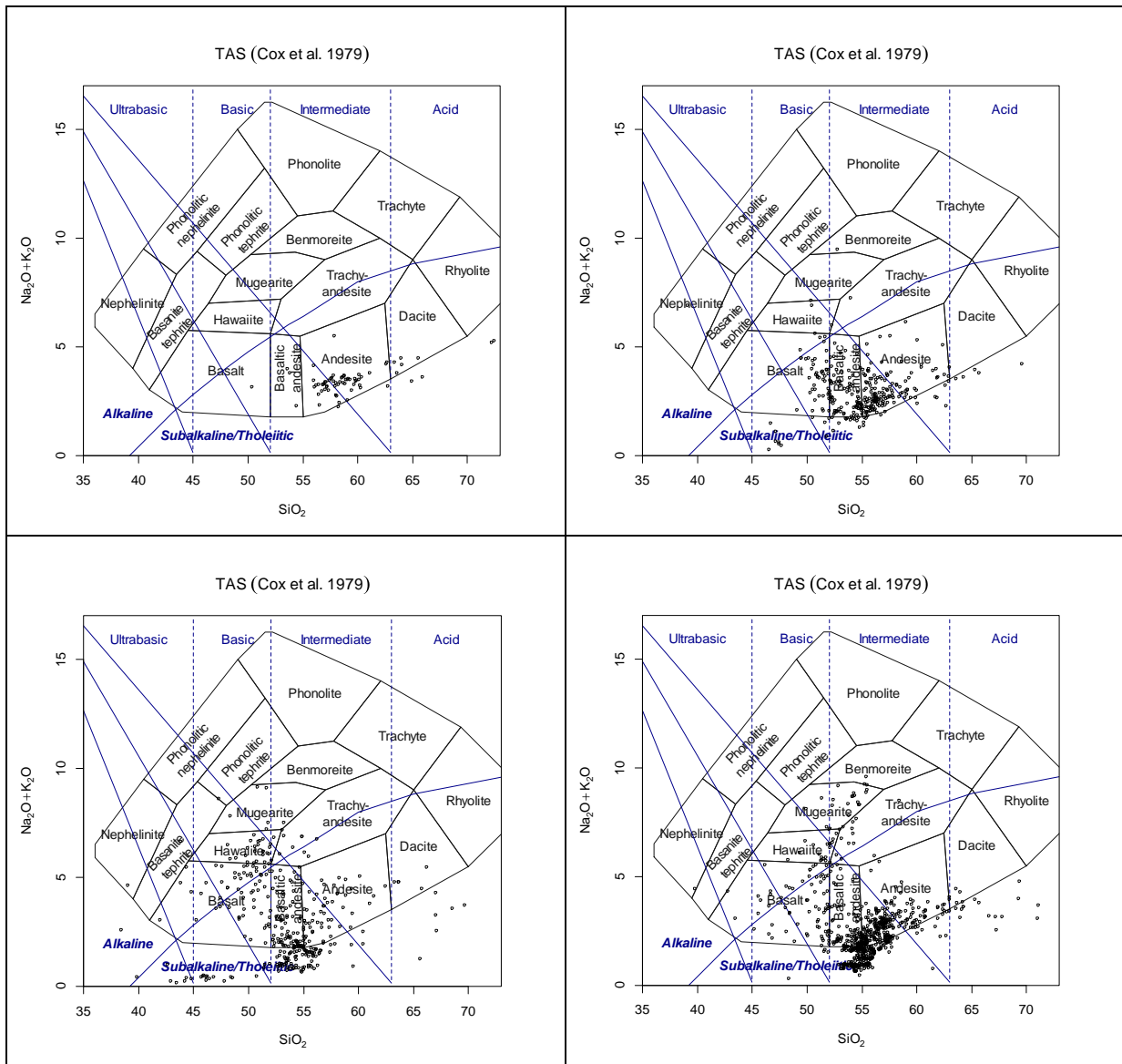


Fig. 5.13-7: Total alkaline silica diagram (COX, K.G., et al. 1979) for samples of the Basal Group, upper left; Lower Pillow Lavas, upper right; Upper Pillow Lava Series, lower left; and the Volcanic Series undifferentiated, lower right. Source of data is given in [table 5.13-2](#). Ideally, there should be a trend from less differentiated samples in the lower left to higher differentiated samples in the upper right - or perpendicularly from the lower right towards the upper left depicting partial melting. Neither the former nor the latter is evident from the plots. At least for samples below / outside the framing line a loss of alkalis is plausible.

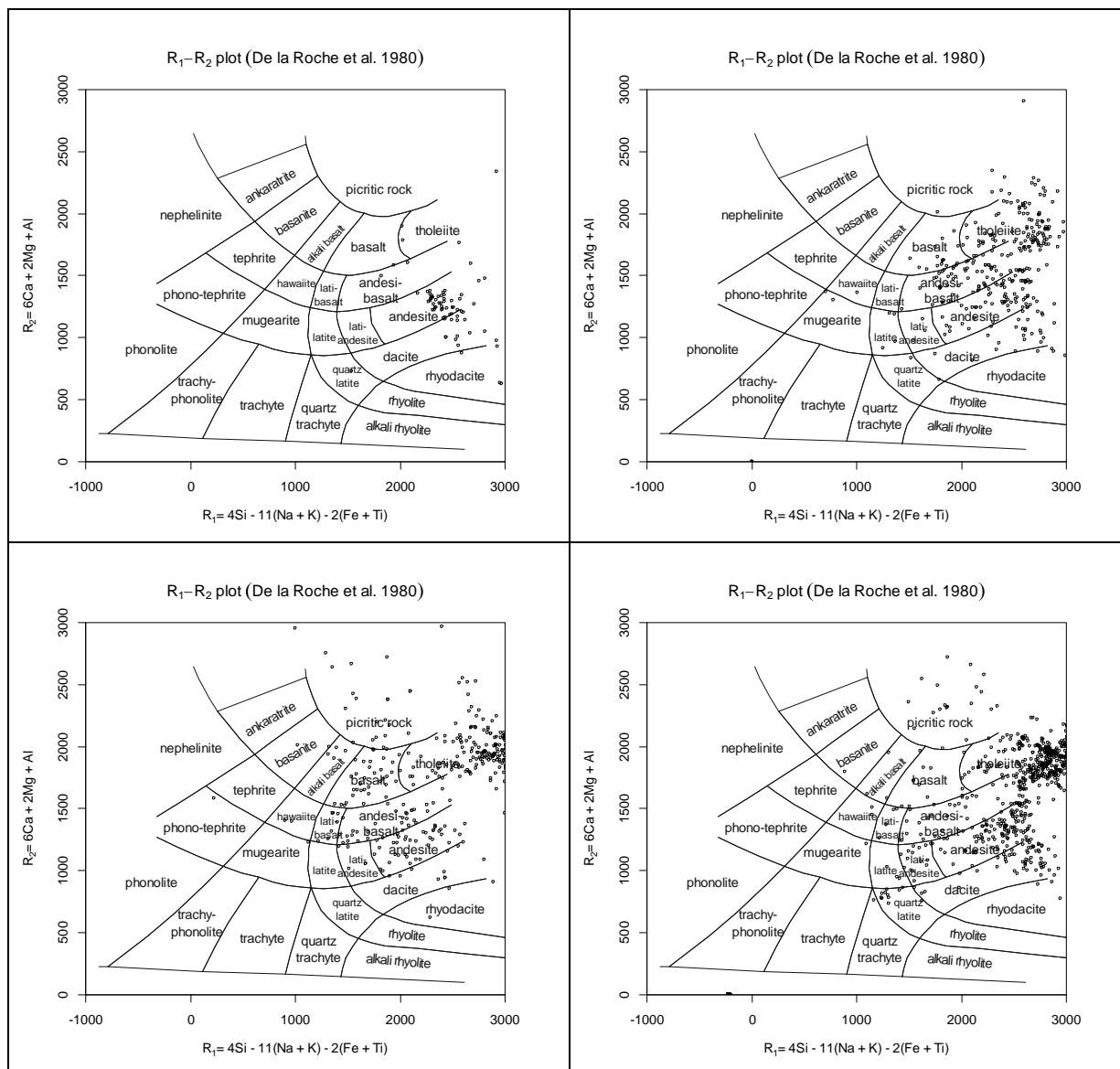


Fig. 5.13-8: R₁-R₂ diagram after (ROCHE, H.D.L. & LETERRIER, J. 1980) used for classification of samples of the Basal Group, upper left; Lower Pillow Lavas, upper right; Upper Pillow Lava Series, lower left; and the Volcanic Series undifferentiated, lower right. Source of data is given in [table 5.13-2](#).

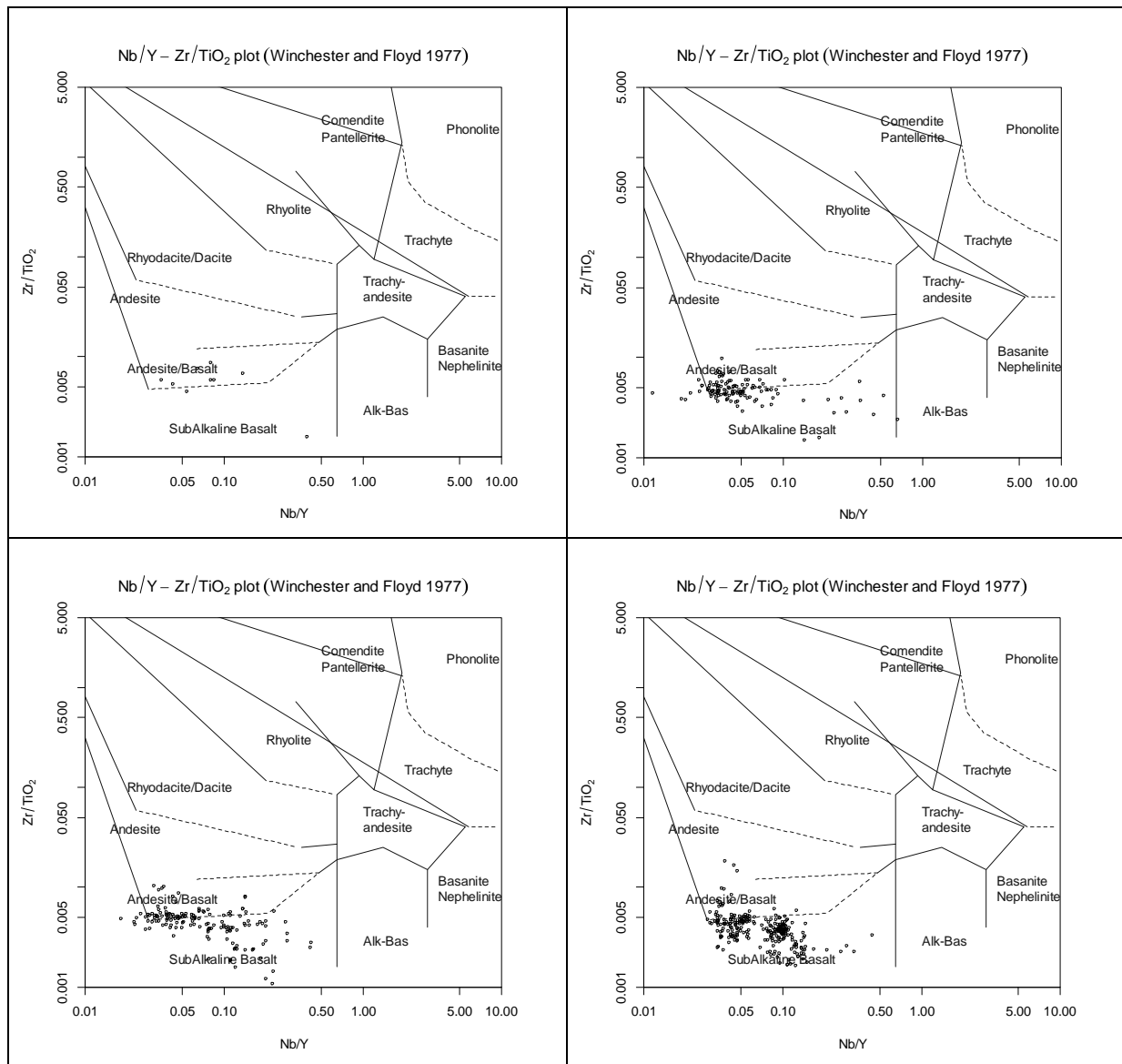


Fig. 5.13-9: Diagram with ratios of incompatible elements Nb and Y against more compatible elements Zr and Ti (COX, K.G., et al. 1979) used for classification of samples of the Basal Group, upper left, unfortunately not many datasets provide all of these four parameters; Lower Pillow Lavas, upper right; Upper Pillow Lava Series, lower left; and the Volcanic Series undifferentiated, lower right. Source of data is given in [table 5.13-2](#).

[Back](#)

5.13.3. Petrogenesis of magmatic rocks of Troodos Ophiolite

Outside of areas with subduction of water-bearing oceanic crust, rocks of the upper mantle consist of almost water-free lherzolite composed of olivine and pyroxenes, see [fig. 5.13-3](#), with additional < 10 vol.-% of aluminosilicates: At > 75 km depth there is garnet present, at 75-30 km spinell and below 30 km plagioclase. Median normative plagioclase content of 23 lherzolite samples from Troodos Massif is 7.4 vol.-%, which means that they originated in a mantle region less than 30 km deep. Under a spreading center where oceanic crust is formed at fast or intermediate rates > 5cm / yr (FRISCH, W. & MESCHÉDE, M. 2005) the upper mantle is of harzburgite composition. This is assumed also for the Upper Cretaceous spreading conditions in the area of present Troodos Massif (NICOLAS, A. 1995), p. 104. In mantle areas with an upward flow direction of heat and material as part of a convection cell partial melting

takes place. This leads to an extraction and ascent of gabbroic/basaltic melt of roughly diopside composition of a few vol.-%, leaving a lherzolite depleted in the clinopyroxene diopside that melts at lower temperatures compared to olivine and orthopyroxene. As a melt is of lower density compared to the solid parent material the molten material moves upwards within the mantle. Further partial melting up to about 20 vol.-% results in more extraction of clinopyroxene and formation of harzburgite and finally residual dunite close to the mantle / crust boundary or Mohorovicic discontinuity (NICOLAS, A. 1995). The so-called Moho is a transition zone where seismic p-wave velocity decreases from > 8 km/s in the mantle to < 8 km/s in the lower oceanic crust, associated with a density change from ca. 3.2-3.3 g/ccm in the mantle to ca. 3.0 in the lower oceanic crust that in total is of gabbroic composition (FRISCH, W. & MESCHEDE, M. 2005). A magma chamber with flancs in the shape of an inverted V and a consequently upwards bent Moho underlies the oceanic ridge at about 5-10 km depth.

During melt ascent cooling at the contact surface to the surrounding crustal material takes place, resulting in crystallisation of different minerals at specific pressure / temperature conditions = fractionated crystallisation. The fabric of a rock provides information about the sequence of crystallisation that usually follows the Bowen reaction series of crystallisation in a melt, see e.g. https://4.bp.blogspot.com/-s1_HG3CklWQ/VAiX01gx_7I/AAAAAAAAABIs/R_1tSI4R9Q/s1600/BowensReactionSeries.jpg. With decreasing temperatures within a melt, solidified material can be ascribed to

1. a discontinuous series starting with Mg- and Fe-rich water-free mafic or dark minerals like olivine, spinell, $MgAl_2O_4$, and chromite, somewhat later pyroxene solidifies, followed by water-bearing amphibole and finally biotite, a dark mica, $K(Mg, Fe^{2+}, Al)_3Al(Si, Al)_3O_{10}(OH)_2$, and
2. a continuous plagioclase, $(Na, Ca)Al(Al, Si)_2Si_2O_8$, feldspar series starting with Ca-rich anorthite, $CaAlSi_2O_8$, and ending with Na-rich albite, $NaAlSi_3O_8$, and
3. late crystallisation of Si- and Al-rich, felsic or light minerals as the K-rich feldspar orthoclase, $(K, Na)AlSi_3O_8$, also named alkalifeldspar or just kalifeldspar, and muscovite, a light mica, $KAl_2(Si_3Al)O_{10}(OH, F)_2$, and finally quartz, SiO_2 .

Quartz forms only in Si-saturated melts, together with feldspars like orthoclase, plagioclase, whereas foids like nepheline, $(Na, K)AlSiO_4$, and leucite, $KAlSi_2O_6$, form if the melt is Si-undersaturated. Foids are a mineral group similar in composition to feldspars but with less SiO_2 content.

Within a magma chamber, solidified minerals tend to sink as they have a higher density compared to the melt: early-crystallised mafic minerals form so-called cumulates at the bottom of the chamber, mainly consisting of olivine, pyroxene and anorthite. It may be difficult to separate between residual underplated uppermost mantle rocks and plutonic cumulates formed in a magma chamber somewhat higher in the lower crust. Cumulates at the Moho can act as a mesh with respect to rising melt, resulting in retention of further early-solidifying minerals like chromite and probably by that process (FRISCH, W. & MESCHEDE, M. 2005) chromite ores on Cyprus have formed, within ultramafic dunite and harzburgite. Median normative chromite content of 5 chromitites of Troodos Massif is 66 vol.-%, that of 25 harzburgites is 0.3 vol.-% and that of 26 dunites 0.47 vol.-%.

Fractional crystallisation changes the chemical composition of the remaining melt. Resulting disequilibrium forces interactions between melt and formerly solidified crystals, reflected e.g. in zoned crystals of plagioclase, usually with an anorthite-rich core and less anorthite-rich margins. The remaining melt increases in Si and Al and decreases in Mg and Fe content. As a consequence, first ultramafic, then mafic, intermediate and finally felsic plutonic rocks form. During all stages of fractionated crystallisation subvolumes of the melt may ascent further upwards forming subvolcanic dykes and volcanic lavas.

Divalent Fe, Mg and Ca cations form part of the so-called compatible elements, they are incorporated into early-crystallised olivine, ortho- and clinopyroxene, see e.g. (SALMINEN, R. 2005). Ions with a larger charge to radius ratio get enriched in the remaining melt, these are the so-called incompatible elements like Rb or Cs. In addition to alkaline elements they are incorporated into amphibole and orthoclase and further minerals like apatite or zircon.

It must be stated that this short overview is a strong simplification, as tectonic movements can induce: shearing of minerals, local melting processes during pressure-release, magma mixing from different melt reservoirs, hydrothermal autometamorphosis by access of water through cracks of the oceanic crust, and at a larger scale mantle heterogeneities will further complicate the formation of real magmatic rock suites, see e.g. (WILSON, M. 1989).

[Back](#)

5.13.4. Plate tectonic milieu interpreted from geochemical analysis of Troodos Ophiolite

As it became evident in chapter 5.13.2, there exists a huge amount of geochemical analyses of rocks from the Troodos ophiolite complex, see [table 5.13-2](#). Including data from the GEOROC database, a total number of 2522 analyses could be retrieved from literature. Beyond these, a few tens of analyses in duplicate were found and the analysis that was published first was taken as the more reliable dataset. In several cases major and minor element contents for the same sample denomination but of different publications were used to form a composite analysis dataset, if major element contents were equal or at least almost equal.

Immobile element ratios can be used to interpret the geotectonic situation under which igneous rocks were formed. In the following, few diagrams were created for samples of the Volcanic Series, undifferentiated, of Troodos Massif, as within this series rocks with the lowest degree of alteration were reported, see e.g. (WÖLKI, D., REGELOUS, M., et al. 2019).

In the ternary $\text{FeO}_{\text{total}}\text{-MgO-Al}_2\text{O}_3$ diagram of (PEARCE, J.A. 1976) samples of the Volcanic Series undiff. fall into all designated fields: Continental Rift, CR, Spreading Center Island or evolved MORB, Island and Continental Arc, IA, MORB; this diagram is not shown.

In the Ti-Zr plot of (PEARCE, J.A. 1982) samples are distributed in the fields Island Arc lavas and MORB and outside these fields; not shown.

In the ternary diagram $2\text{Nb-Zr}/4\text{-Y}$ for basaltic rocks after (MESCHÉDE, M. 1986) most samples fall into the field of normal MORB, Mid-Ocean Ridge Basalts, but a considerable part of the samples lies outside any denominated field; not shown.

In diagrams of (PEARCE, J.A. & MCCANN, J.R. 1973): 1. $\text{Ti}/100\text{-Zr-}3\text{Y}$, 2. $\text{Ti}/100\text{-Zr-Sr}/2$, 3. Zr versus Ti, samples are spread 1. in the fields Island-arc tholeiites, IAT, MORB & IAT and outside designated fields, 2. in MORB, IAT and Calc-alkaline basalts, CAB, and again outside of these fields, 3. most fall into the field of IAT, some into MORB & CAB & IAT, CAB, MORB and again outside of any field; not shown.

In the Zr versus Zr/Y diagram of (PEARCE, J.A. & NORRY, M.J. 1979) samples plot in the Island Arc Basalts, IAB, and MORB fields, but many outliers are present as well; not shown.

In the ternary diagrams 1. $\text{Hf}/3\text{-Th-Ta}$, 2. $\text{Hf}/3\text{-Th-Nb}/16$, $\text{Zr}/117\text{-Th-Nb}/16$ of (WOOD, D.A., et al. 1979) samples plot in all of the following fields: normal-MORB, evolved-MORB, within-plate basalts, CAB and IAT; not shown.

In the ternary plot $\text{TiO}_2\text{-}10\text{MnO-}10\text{P}_2\text{O}_5$ (MULLEN, E.D. 1983) samples plot in all fields: Boninit/CAB, IAT, MORB, Ocean Island Tholeiite, OIT, with the exception of Ocean Island Alkalibasalts, OIA; not shown.

In [fig. 5.13-10](#) samples plot in the Th/Nb versus La/Yb diagram of (HOLLOCHER, K. 2012) in the Oceanic Arcs field, in the La/Yb versus Nb/La diagram both in the Oceanic Arcs and MORB fields. This diagram is shown as an example of the variability of the samples from Troodos Massif Volcanic Series undiff..

To the opinion of the authors, plots of major and trace elements from literature data for Troodos Massif do not allow an explicit statement about the plate-tectonic regime in Cretaceous time under which the rocks of the Volcanic Series have formed, as the samples plot in different fields in different diagrams. There are however interpretations of the structural situation, only newer literature is presented here: from geochemical data (REGELOUS, M., et al. 2014) assumed a triple junction, i.e. a zone where three plates adjoin, (WÖLKI, D., REGELOUS, M., et al. 2019) interpreted a supra-subduction back-arc spreading center at a triple junction. From the orientation of dykes in the Sheeted Dyke Complex (MORRIS, A. & MAFFIONE, M. 2016) also argued for a segment of an oceanic ridge bound by a transform-fault, i.e. also a triple-junction.

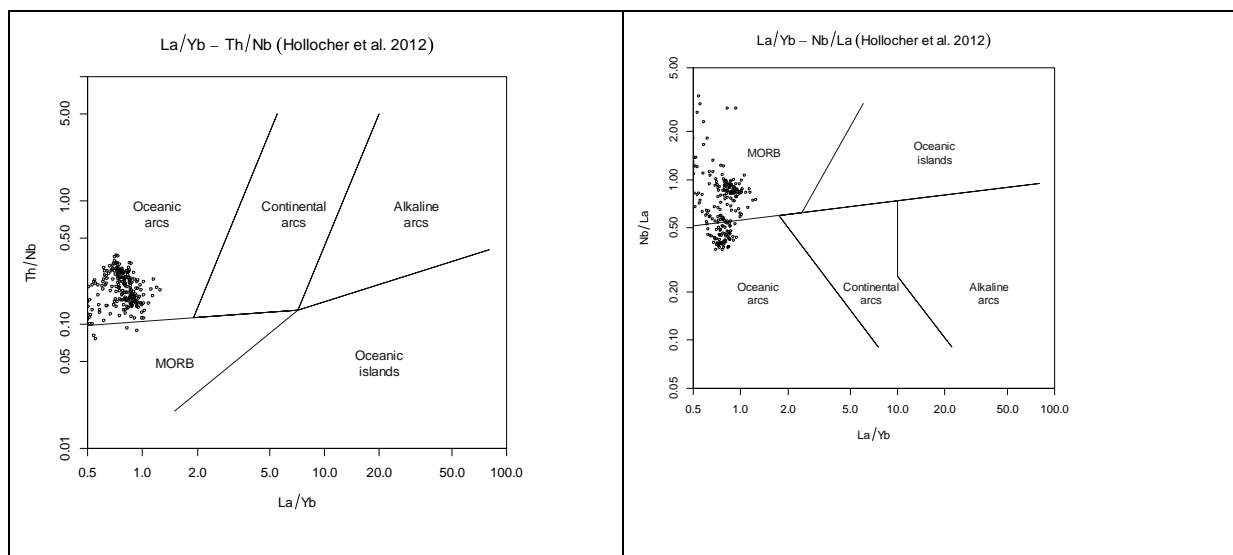


Fig. 5.13-10: Plots of geochemical data for the Volcanic Series undiff., for references see [table 5.13-2](#), in diagrams constructed for the allocation of magmatic rocks to plate tectonic regimes by (HOLLOCHER, K. 2012).

[Back](#)

5.13.5. Magnetic susceptibility of whole rocks from Cyprus

For the measurement of mass-specific magnetic susceptibility, MS , at a frequency of 460 Hz a Bartington MS2 susceptibility meter with sensor B has been used, following procedures described in (DEARING, J. 1994). Drift corrected values measured in the cgs system were transformed into SI values [$10^{-9} \text{ m}^3 \text{ kg}^{-1}$]. In addition, the frequency-dependancy of magnetic susceptibility, MS_{fd} , was measured at 460 and 4600 Hz, see (DEARING, J.A., et al. 1996), for samples where the drift-corrected raw readings where $> 20 [10^{-6} \text{ cgs}]$.

In total 74 samples were available from outcrops in 2019, from a petrographical kit of the Geological Survey of Cyprus or were provided by MICHAEL ONISIFOROU for this study, for a detailed list see [table 5.13-3](#).

Within Troodos Massif, ultramafic wehrlite is the rock with the highest median MS value and sulfide ores are those with the lowest MS value. The first observation may be also helpful in geological mapping, as in case of serpentinization ultramafic rocks may be difficult to differentiate in the field, in addition to the already mentioned problem in assigning opx or cpx. Serpentinite rocks from Troodos Massif reveal a large variability from 169 to 12900 [$10^{-9} \text{ m}^3\text{kg}^{-1}$]. Compared to fresh ultramafites it is obvious that this variability is comparable to the range of MS values of possible educts with the exception of wehrlite. Chromite, harzburgite and pyroxenite reveal lower than average MS values. For the mapping of chromitite in the field this might be of economic interest, but such an observation should be supported by further data.

MS_{fd} , an indicator for superparamagnetic particles of a grain size $< 0.1 \mu\text{m}$ (EVANS, M.E. & HELLER, F. 2003), is $< 3 \%$ for most rocks studied here. In [fig. 5.13-11](#) MS and MS_{fd} are plotted against one another, both parameters do not correlate. For the majority of rocks the presence of superparamagnetic magnetite can be excluded and magnetite should occur in larger single-, pseudo-single and multidomain grain sizes, see e.g. (EVANS, M.E. & HELLER, F. 2003). As crystal size is dependent from cooling rates this may be an argument for slow cooling. This however cannot be assumed for pillow lavas directly in contact with sea water. Hence, magnetite crystals in Lower and Upper Pillow Lava Series should have crystallised at somewhat larger depth. Higher MS_{fd} values could result from oxidation of divalent iron in soils by e.g. forest fires or redoxomorph conditions in valleys, see e.g. (DEARING, J.A., et al. 1996). But as the samples of this study are more or less fresh this is not to expect for most of the material inspected in this study. Somewhat higher values of 4 to 7 % MS_{fd} in umber and chromitite indicate an intermediate content of ultrafine superparamagnetic magnetite. For umber this probably resulted from relatively fast crystallisation at the contact of melt with sea water. For chromitite this may have resulted from exsolution processes. Composition of both rocks is far from that of the other rocks, as they contain low to very low silica, $< 1 \text{ wt.}\%$ for chromitite and around 35 wt.-% for umber. For both rocks a calculation of CIPW norms does certainly not provide realistic normative mineral compositions. This assumption is supported by the high normative magnetite content of umber: ca. 35 vol.-% magnetite and 28 wt.-% of hematite, Fe_2O_3 . The former value cannot be correct after comparison with the low MS values observed. However, the occurrence of ultrafine magnetite in creek sediments could be an evidence for the presence of chromite ores or umber in a catchment.

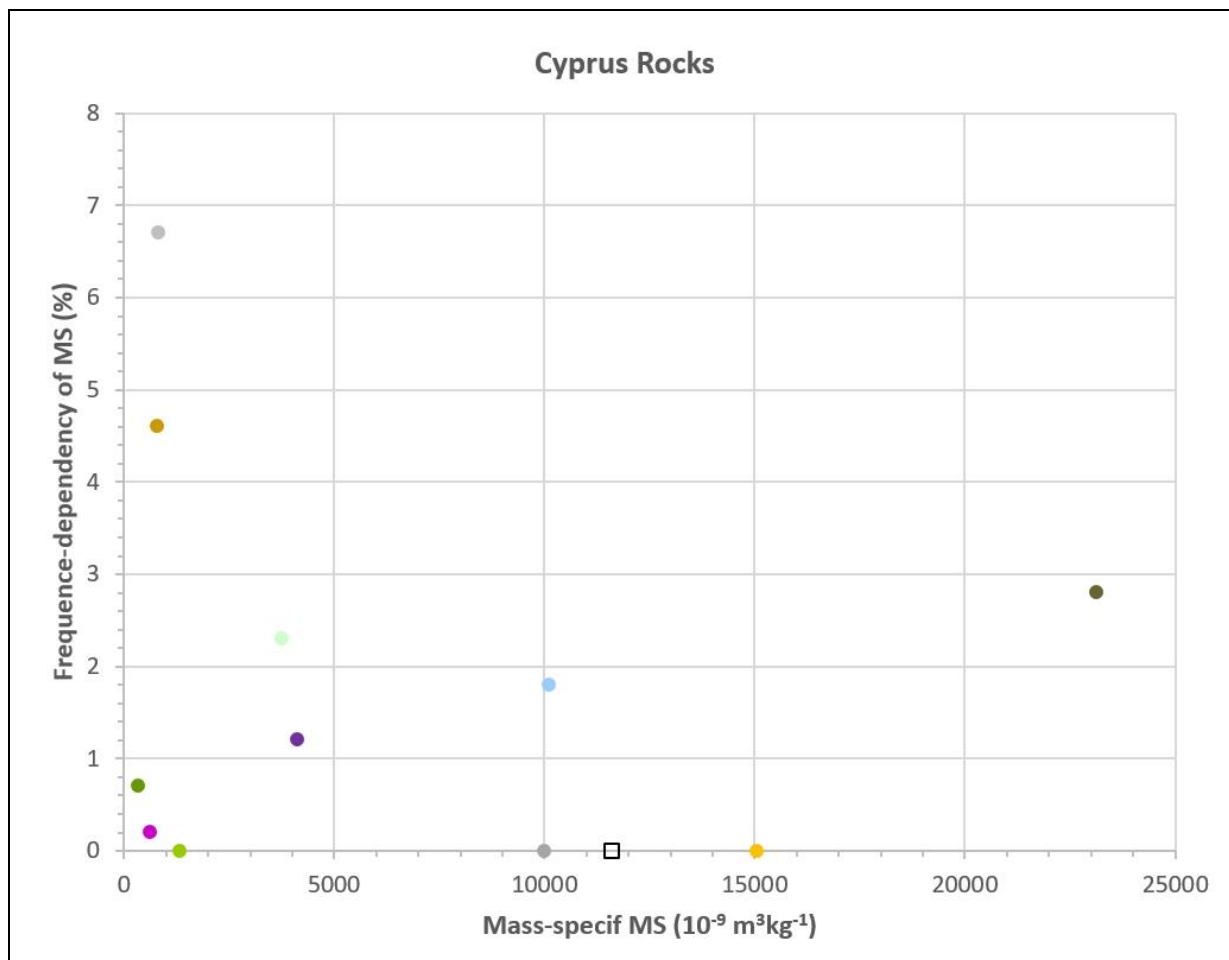


Fig. 5.13-11: Mass-specific magnetic susceptibility plotted against frequency-dependency of MS. The square symbol marks recent river sediments, for colours of the other symbols see [table 5.13-2](#). Error bars or confidence levels are not shown for clarity, for MS the latter are presented in [figs. 5.13-12](#) and [-13](#) and for frequency-dependency the standard deviation is in the order of 0.5 to 1.5 %.

Two samples of recent sediments from rivers discharging diabase and volcanics of the Troodos Massif have high values of MS, which could result from placer forming processes by fluvial transport. In contrast, three recent litoral sediments of the Mediterranean Sea have only intermediate MS values as they represent a mixture of mafic and ultramafic rocks with diamagnetic carbonatic debris produced from reworking of shells and skeletons. Nevertheless, due to the high portion of ultramafic and mafic rocks the latter values are higher than e.g. that of the litoral Mediterranean in southern France (PIRRUNG, M., et al. 2017).

Tab. 5.13-3: Mass-specific magnetic susceptibility, MS, in [10^{-9} m³kg⁻¹], and frequency-dependency of MS, MS_{fd} in [%], determined on whole rocks in this study. N = number of samples measured. The samples are arranged from young to old and with increasing crustal depth of the lithological units. CGS = samples from petrographical kit of Cyprus Geological Survey, all taken within Troodos Massif. MO = sample from MICHAEL ONISIFOROU, Nicosia. GP = site of Troodos Geopark, GPM = Mine of Troodos Geopark; ED = stop of (EDWARDS, S., et al. 2010). The MS color coding is similar to that of [fig. 5.13-1](#): <100, 100-499, 500-999, 1000-10000, >10000.

Lithostratigraphy	Rock type	Location	N	MS	MS _{fd}
Recent	River sand	Akaki River, W'ED3.10; Loumata River, E'ED7.18	2	11598	0.0
Recent	Beach sand	Governors Beach, Mare-Med19-4; Larnaca Mare-Med19-5, -6	3	2480	0.0
Roman	Slag	Scouriotissa, GPM6, ED7.3	1	4384	1.0
Eocene	Chalk-like limestone, very light beige; chert, grey Chert, grey	Governors Beach, ED6.6a	2	9	
Upper Cretaceous	Umber, Dark brown siltstone	CGS	3	801	4.6
Upper Pillow Lavas	Picrite Basalt Olivine Basalt Ochre Jasper with hematite Sulfidic ore	CGS CGS CGS Mitsero Mine, GPM3, ED7.4 CGS; Mathiatis Mine, ED3.15	3 4 3 1 4	215 6415 309 274 22	1.9 2.3 2.5 22.0
Lower Pillow Lavas	Andesite-Dacite	CGS	4	10117	1.8
Dyke Complex	Diabase Light dyke	CGS; W'Palaichori, GP33; SW'Klirou, ED3.10 SW' Troodos, GP39&ED2.7-1	5 1	9988 105	0.0
Plutonic sequence	Plagiogranite Gabbro Pyroxenite Wehrlite	CGS; W'Palaichori, GP33 CGS, SW' Troodos, GP39&ED2.7-1 CGS; MO: Atalante & Artemis Trails CGS; SW' Troodos, GP39&ED2.7-1; MO: GP7	3+1 3 5+2 3+1+1	15059 1339 346 23145	0.0 0.0 0.7 1.0
Mantle sequence	Dunite Chromitite Serpentinite Harzburgite	CGS; MO: Artemis Trail CGS; Kannoures Mine, GPM10&ED2.3 CGS; S'Troodos, N'GP6; Amiantos, GPM11&ED7.18 CGS; MO: Artemis Trail	4+1 3+1 3+1+1 3+2	4122 814 7722 632	1.2 6.7 0.0 0.2

In an aeromagnetic map of Cyprus, see also (VINE, F.J., et al. 1973), very high total magnetic intensity anomalies, reduced to the north-pole (PAPADOPOULOS, N.G., et al. 2005), are present on the northern slopes of Troodos Massif, where the Lower and Upper Pillow Lava Series are widespread. Samples from the Lower Pillow Lava Series show the third-highest MS measured on Troodos Massif samples, see [table 5.13-3](#). Only one additional area with very high values is observable on the southwestern slopes, located near the village of Philousa, where Lefcara Formation sediments are widespread besides a southward extension of Upper Pillow Lava Series (PANTAZIS, T. 1979). This indicates that the lavas continue under their sedimentary cover at several tens of meters depth. The central part of mantle rocks with serpentinite, harzburgite and dunite around Troodos Village is characterized by very low total intensity values. This might point to a loss of magnetominerals under low pressure conditions, whereas many studies demonstrate the formation of magnetite during serpentinisation, e.g. in the Alps.

(MELCHER, F., et al. 2002). However, there is a narrow NE-striking zone to the west of Prodhromo, which is located about 5 km west of Troodos Village. Here relatively high total magnetic intensity values coincide with a plagiogranite intrusion into gabbros, elongated in approximately the same direction. Plagiogranite samples have the second highest MS observed in measurements of this study. The high magnetic values imply that this intrusion is somewhat larger at depth compared to surface outcrops. Patches of wehrlite, the rock with highest MS measured on Troodos Massif samples, surrounding the mantle rock zone (PANTAZIS, T. 1979), do not coincide with high aeromagnetic anomalies. This means that these occurrences may be too small for aeromagnetic detection at the flight height which was around 2600 m a.s.l., at least 650 m above ground level. For the interpretation of aeromagnetic anomalies (PAPADOPOULOS, N.G., et al. 2005), p. 60, used an average volume-specific MS of 0.025 [SI], or 25000 [10^{-6} SI], for Troodos Ophiolite igneous rocks, but they did not indicate if this was just an assumption from literature data or if own results were available. If the aerial distribution of different rock types, estimated from (PANTAZIS, T. 1979), in Troodos Massif including the Limassol Forest area south of Arakapas Fault, southeast of Troodos Massif, see [table 5.13-4](#), is used to calculate area-weighted density and MS values, then results for volume-specific MS are in relatively good accord with the value assumed by (PAPADOPOULOS, N.G., et al. 2005)!

The area-weighted density in [table 5.13-4](#) is close to the value of 3.0 g/ccm measured for average oceanic crust, see e.g. <https://joidesresolution.org/wp-content/uploads/2018/03/Ocean-Crust-Density.pdf>. From seismic and gravity data (MACKENZIE, G.D., et al. 2006) assumed a density of 2.21 g/ccm for sediments and Upper Pillow Lava Series, 2.31 g/ccm for Lower Pillow Lava Series and Basal Group, 2.72 g/ccm for Sheeted Dyke Series, 2.92 g/ccm for gabbros, 3.0 g/ccm for cumulates and peridotite. These densities are significantly lower than those presented in table 5.13-4. However, they did not result from direct density measurements but from modeling of seismic and gravity data. (HUNT, C.P., et al. 1995) published an average density of gabbro that is identical to that in [table 5.13-4](#) and for peridotite of 3.15, at least somewhat higher than the value used by (MACKENZIE, G.D., et al. 2006). (NICOLAS, A. 1995), p. 120, postulated a density of 3.3 g/ccm for upper mantle peridotite. In addition, the value for basalts given by (HUNT, C.P., et al. 1995) is identical to that for the Upper Pillow Lava Series estimated from normative mineral composition in this study. As a consequence the modelled depths of boundaries of structural units presented by (MACKENZIE, G.D., et al. 2006) should be regarded as just one possible interpretation.

Tab. 5.13-4: Roughly estimated aerial distribution of ophiolite rocks in Cyprus, based upon (PANTAZIS, T. 1979), density calculated from CIPW norm of literature data, see [table 5.13-2](#), mass-spec. MS and estimated vol.-spec. MS using the density values of this table. Numbers in *italic* are assumed from adjacent stratigraphic units. Given density of the lowest unit does not consider serpentinisation.

Lithostratigraphical Series	Area [%]	Density [g/ccm]	Mass-spec. MS [10 ⁻⁹ m ³ kg ⁻¹]	Vol.-spec. MS [10 ⁻⁶ SI]
Upper Pillow Lava Series	5	2.99	5418	16190
Lower Pillow Lava Series	10	2.96	10117	29979
Basal Group	10	2.93	<i>10000</i>	<i>29300</i>
Sheeted Dyke Series	50	2.95	9988	29444
Plagiogranite	5	2.78	15059	41803
Gabbro	9	3.03	1339	4063
Pyroxenite	1	3.25	346	1123
Wehrlite	1	3.3	21456	70805
Dunite	1	3.32	4122	13696
Partly serpentinized Harzburgite	8	3.31	632	2094
Sum / area-weighted average	100	2.99	8460	24939

[Back](#)

5.13.6 Geochemistry and magnetic susceptibility

In most rocks magnetic susceptibility is dominated by the occurrence of ferrimagnetic minerals (THOMPSON, R. & OLDFIELD, F. 1986). In unaltered igneous rocks magnetite, Fe₃O₄ or written as Fe²⁺O + Fe³⁺₂O₃, and ulvöspinell, Fe²⁺₂TiO₄, form a solid-solution series named Ti-magnetite (EVANS, M.E. & HELLER, F. 2003), that represents the most important minerals concerning rock magnetism, besides hematite und ilmenite with much lower MS. The MS measurements thus provide an opportunity to test if the calculated CIPW-normative mineral content is realistic for magnetite content. For the calculation of normative magnetite, hematite, ilmenite only individual analyses were used, no medians or means. If the latter values would be used, too high Fe-contents would result as not all samples contain Fe₂O₃ and FeO, but most contain either Fe₂O_{3total} or FeO_{total} and using both medians would produce erroneous mineral compositions.

In [fig. 5.13-12](#) there is a relatively convincing positive correlation between normative magnetite and mass-spec. MS, although the CIPW norm only considers pure magnetite without Ti content. This supports the assumed Fe³⁺/Fe_{tot} ratios for most rock samples measured in this study. There is however one outlier, not shown in [fig. 5.13-12](#): for umber a calculated mt content of ca. 35 vol.-% does not fit to the observed mass-spec. MS of only 801 [10⁻⁹ m³kg⁻¹]. For umber a higher hematite content can be expected than the calculated ca. 28 vol.-% of normative hematite.

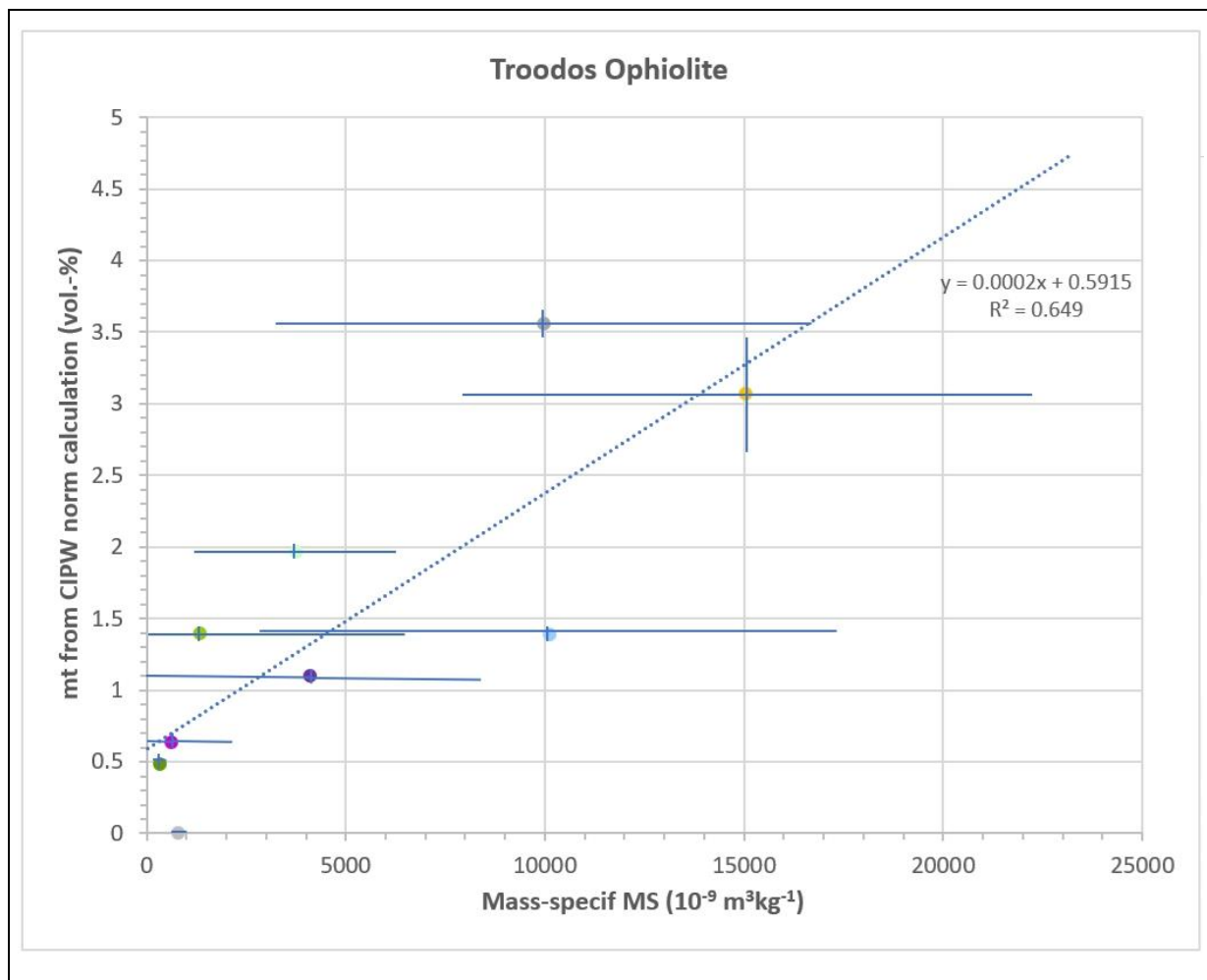


Fig. 5.13-12: Correlation between mass-specific MS for igneous rocks from Troodos Massif, measured in this study, see [table 5.13-3](#) and normative magnetite content, mt, calculated from published analyses, for references see [table 5.13-2](#); for symbol colours see [table 5.13-1](#), for both parameters the 95 % confidence intervals are shown, some of them were cut off at the ordinate axis.

A correlation between median FeO or Fe₂O₃ content is not shown, as Fe is a component in many minerals besides magnetite, ilmenite and hematite, e.g. in pyroxenes, amphiboles, biotite, pyrite. As average oceanic crust contains Ti-magnetite of the composition Fe_{2.4}Ti_{0.6}O₄, also named TM60 (EVANS, M.E. & HELLER, F. 2003), p. 36, TiO₂ content may be an indicator for the presence of Ti-magnetite. In [fig. 5.13-13](#) the positive correlation between median values for mass-spec. MS versus Ti-content for magmatic rock types of the Troodos Massif is marked by a somewhat lower squared linear correlation coefficient, r^2 , compared to that in [fig. 5.13-12](#). This is not surprising if we take into account the occurrence of Ti in other minerals as ilmenite, present as normative mineral in most igneous rocks from Troodos Massif in low amounts, and rutile, rarely present as normative mineral in these rocks, but also in clinopyroxene, like Ti-augite, not calculated in CIPW norm.

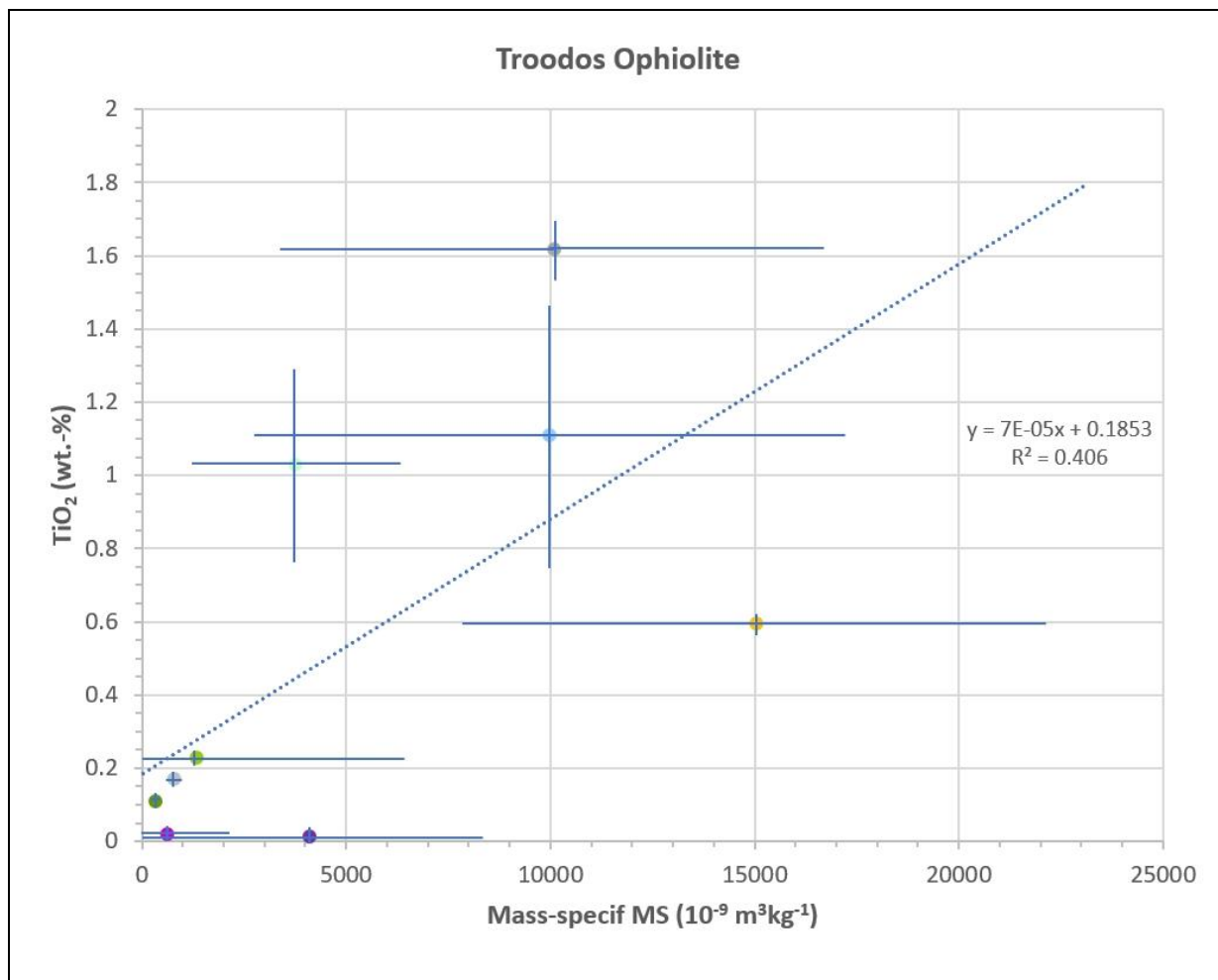


Fig. 5.13-13: Correlation between median mass-specific MS for rock types of Troodos Massif measured in this study, see [table 5.13-3](#), and median TiO₂-content, for references see [table 5.13-2](#), for symbol colours see [table 5.13-1](#), 95 % confidence intervals are shown.

In the Sheeted Dyke Series, altered by greenschist grade metamorphism, (VARGA, R.J., et al. 1999) reported local replacement of primary magnetite by secondary sphene, also called titanite, CaTiSiO₅, and alteration to secondary hematite and maghemite. The same authors reported Curie temperatures of 585 °C, which indicate presence of pure magnetite, and changes in thermomagnetic curves characteristic for maghemite/hematite conversion. From anisotropy measurements of MS and thermomagnetic magnetization and demagnetization curves (BORRADAILE, G.J. & GAUTHIER, D. 2006) postulated the occurrence of both magnetite and Ti-magnetite for the Sheeted Dyke Series. For the lower part of the Volcanic Series and the Sheeted Dyke Series (HALL, J.M., et al. 1995) suggested replacement of primary Ti-magnetite by neoformation of secondary stoichiometric magnetite and exsolution of Ti-rich phases like ilmenite during hydrothermal alteration. From thermomagnetic magnetization and demagnetization curves of samples from gabbros from Troodos Massif (GRANOT, R., et al. 2007) supposed presence of low-Ti Ti-magnetite. In pyroxenes of gabbros (EBERT, Y., et al. 2010) observed inclusions of pyrrhotite, Fe_{1-x}S with 0 < x < 0.2, pure magnetite and rare Ti-magnetite and interpreted exsolution of magnetite from pyroxene during magma solidification. Another source of magnetite formation might be serpentinization of ultrabasic rocks (BEARD, J.S., et al. 2009). The relatively high value of mass-spec. MS of four serpentinite samples in Troodos Massif in comparison to less or not serpentinitised ultramafic parent rock samples, see [table 5.13-3](#), may be considered as argument for serpentinization of olivine in favour of pure magnetite formation at least in mantle rocks from Troodos Massif, possibly also in some altered sheeted dykes.

A schematic overview on selected magnetomineral transformations is presented in [fig. 5.13-14](#), based on thermomagnetic data. Measurements were performed on about 50 mineral samples either in air or under a predominant Ar atmosphere using a Bartington temperature-susceptibility-system at the Institute for Geosciences in Jena. General information for the identification of newly formed minerals from their Curie- and Neel-temperatures, respectively, were taken from (THOMPSON, R. & OLDFIELD, F. 1986) and (EVANS, M.E. & HELLER, F. 2003), together with further sources. The content and oxydation state of Ti in the minerals was not considered, but in principal a similar figure could be constructed.

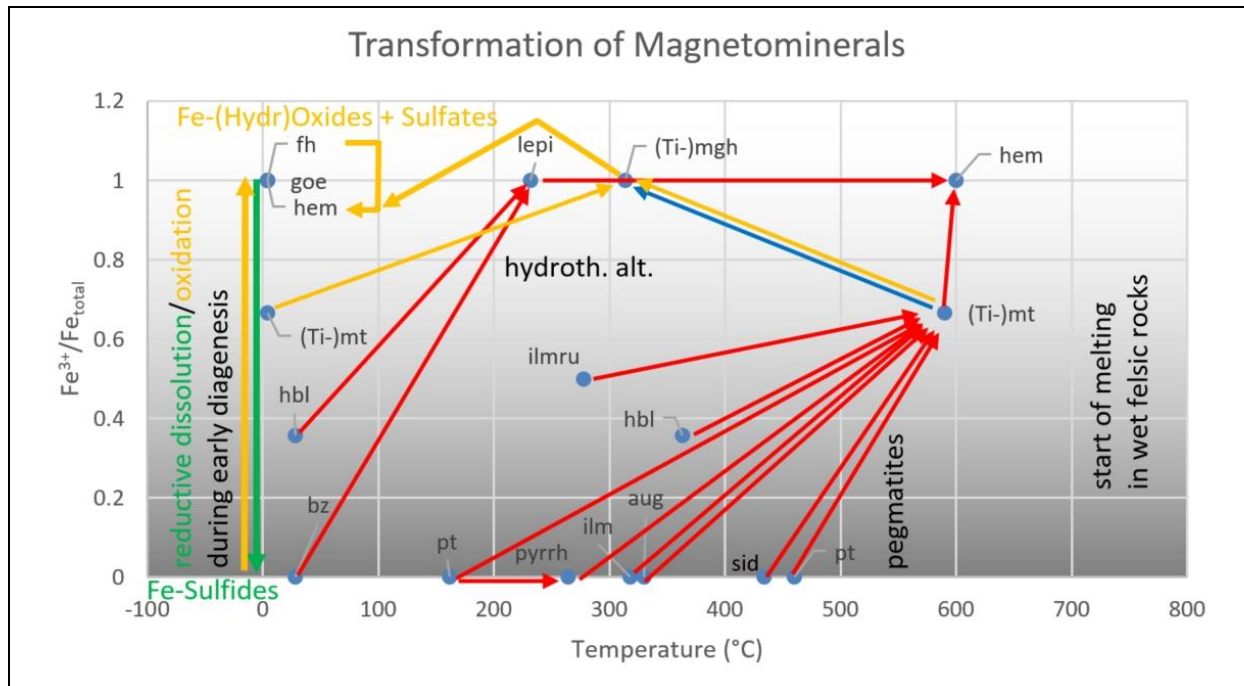


Fig. 5.13-14: Selected Fe-rich minerals and their transformations during changes of redox and temperature conditions. Oxygen fugacity in melts was expressed by the molar Fe^{3+}/Fe_{total} ratio, calculated from formulas given in the Mineral Database (DYAR, M.D., et al. o.a.). Temperatures ranged between room temperature and 800 °C and were registered in steps of 2 °C. Red arrows show reactions during heating, most of these are not reversible within cooling time in the laboratory. Blue dots represent the begin of mineral reactions during heating, evident from changes in magnetic susceptibility of the sample. The blue arrow marks a reaction from magnetite to Ti-Maghemite during cooling after former heating of siderite. The orange arrows represent slow transitions in soils after (MAXBAUER, D.P., et al. 2016). Abbreviations: aug augite, bz bronzite, fh ferrihydrite, goe goethite, hbl hornblende, hem hematite, ilm ilmenite, ilmru ilmenorutile, lepi lepidocrocite, mgh maghemite, mt magnetite, pt pyrite, pyrhh pyrrhotin, sid siderite.

[Back](#)

5.13.7. Summary and outlook

The main results of this study are:

- The Troodos Massif is certainly one of the best investigated Mediterranean ophiolites with a high number of geochemical analyses of its volcanic rocks, whereas from plutonic and mantle rocks only a relatively small amount of analyses is available from literature, see [table 5.13-2](#).
- In literature there are no analyses that can be classified as Wehrlite if CIPW normative mineral contents are plotted in the ternary opx-ol-cpx diagram for ultramafic rocks, see [fig. 5.13-3](#).
- The mantle region under Troodos Massif from which melts rised to form the oceanic crust was less than 30 km deep. The parental plagioclase-bearing lherzolite contains about 20 vol.-% of normative opx, see [fig. 5.13-3](#).
- The gabbroid rocks, that form the major part of the Plutonic Series, see (DILEK, Y. & FURNES, H. 2009), p. 8, are mainly of gabbro-norite composition if CIPW normative mineral content is taken for classification in the ternary diagram opx-plag-cpx for mafic igneous rocks, see [fig. 5.13-4](#).
- About half of the samples from the Sheeted Dyke Series that in the literature are generally classified as diabase consist of microgabbros and quartz gabbros, but another half has to be denominated as tonalites, see [fig. 5.13-5](#), if CIPW normative minerals are used for classification. This indicates an origin from plagiogranite intrusions at least for some of the dykes.
- The majority of plutonic and volcanic rocks of Troodos Ophiolite are silica-saturated, only few samples are undersaturated, see the QAPF diagram in [figs. 5.13-5](#) and [-6](#). This is a consequence of the excessive formation of ultramafic cumulates in the lowermost oceanic crust (DILEK, Y. & FURNES, H. 2009) under a fast spreading ridge (NICOLAS, A. 1995) and consequent enrichment of silica in plugs of ascending melt.
- Alkalies were mobilised during hydrothermal alteration of volcanic rocks and cannot be used for classification, see [figs. 5.13-7](#) and [-8](#). Incompatible elements allow a classification of the majority of volcanics in the fields of subalkaline basalt and andesite/basalt, see [fig. 5.13-9](#).
- Major and trace element discrimination does not allow to attribute igneous Troodos ophiolite rocks to a specific plate tectonic regime, see discussion of several discrimination diagrams not shown and that in [fig. 5.13-10](#).
- Samples of wehrlite have the highest observed magnetic susceptibility of the ophiolite rocks, see [table 5.13-3](#).
- At the available resolution and flight height of aeromagnetic data (PAPADOPOULOS, N.G., et al. 2005) wehrlite rocks are not visible in total magnetic intensity maps due to the small size of outcrops.
- Densities calculated from CIPW norm in this study are higher than those postulated by (MACKENZIE, G.D., et al. 2006) based on geophysical data, but they correspond quite well to values given by (HUNT, C.P., et al. 1995).
- Low values of frequency-dependency of magnetic susceptibility indicate a low content of ultrafine magnetite and thus a subvolcanic region for magnetite crystallisation in pillow lavas, see [fig. 5.13-11](#).

- CIPW normative magnetite of the ophiolite rocks is positively correlated with mass-spec. magnetic susceptibility, see fig. [fig. 5.13-12](#), and to a lower degree with TiO₂ content, see [fig. 5.13-13](#). The former observation can be considered as an argument for realistic Fe³⁺/Fe_{tot} ratios on which the CIPW norm calculation of this study was based. The latter aspect indicates presence of either titanomagnetite or other Ti-bearing minerals.
- Serpentinisation of olivine under greenschist-facies conditions probably contributed to neof ormation of magnetite in some ultramafic rocks, see [table 5.13-3](#).

The impressive outcrops in Cyprus provide a phantastic insight into the composition of a Mediterranean ophiolite. Hopefully during future excursions in cooperation with the Cyprus Geological Survey and the University of Cyprus further samples may be taken for a more detailed analysis. In addition to MS and CIPW norm data, discussed in this study, a determination of Curie temperature may help to identify ferrimagnetic minerals. A publication of magnetic susceptibility and Curie temperature data from Cyprus is planned for a future manuscript.

[Back](#)

5.13.8. References

Selected links to geological maps:

<https://esdac.jrc.ec.europa.eu/images/Eudasm/CY/cypr6.jpg>;
<https://image.jimcdn.com/app/cms/image/transf/dimension=890x10000:format=jpg/path/s43f928e84fd05874/image/if5e0a690e88e2ce0/version/1413307957/geological-map-of-cyprus-geological-survey-department.jpg>;
<https://gsd.maps.arcgis.com/apps/View/index.html?appid=e6f54157fe8640cc853df09bf2e75dd7>

Links to soil maps:

<https://esdac.jrc.ec.europa.eu/images/Eudasm/CY/cypr2-1.jpg>,
<https://esdac.jrc.ec.europa.eu/images/Eudasm/CY/cypr2-2.jpg>,
<https://esdac.jrc.ec.europa.eu/images/Eudasm/CY/cypr5.jpg>

Link for ore mining sites:

<http://homersheimat.de/themen/minen-auf-zypern/images/minen-auf-zypern.jpg>.

- BEARD, J.S., FROST, B.R., FRYER, P., MCCAIG, A., SEARLE, R., ILDEFONSE, B., ZININ, P. & SHARMA, S.K. (2009): Onset and progression of serpentinization and magnetite formation in olivine-rich troctolite from IODP Hole U1309D. *Journal of Petrology*, 50: 387-403.
- BEDNARZ, U. & SCHMINCKE, H.-U. (1994): Petrological and chemical evolution of the northeastern Troodos Extrusive Series, Cyprus. *Journal of Petrology*, 35: 489-523.
- BORRADAILE, G.J. & GAUTHIER, D. (2006): Magnetic studies of magma-supply and sea-floor metamorphism: Troodos ophiolite dikes. *Tectonophysics*, 418: 75-92.
- BÜCHL, A., BRÜGMANN, G. & BATANOVA, V.G. (2004): Formation of podiform chromitite deposits: implications from PGE abundances and Os isotopic compositions of chromites from the Troodos complex, Cyprus. *Chemical Geology*, 208: 217-232.
- BÜCHL, A., BRÜGMANN, G., BATANOVA, V.G., MÜNKER, C. & HOFMANN, A.W. (2002): Melt percolation monitored by Os isotopes and HSE abundances: a case study from the mantle section of the Troodos Ophiolite. *Earth and Planetary Science Letters*, 204: 385-402.
- BÜCHL, A., BRÜGMANN, G.E., BATANOVA, V.G. & HOFMANN, A.W. (2004): Os mobilization during melt percolation: The evolution of Os isotope heterogeneities in the mantle sequence of the Troodos ophiolite, Cyprus. *Geochimica et Cosmochimica Acta*, 68: 3397-3408.
- CAMERON, W.E. (1985): Petrology and origin of primitive lavas from the Troodos ophiolite, Cyprus. *Contributions to Mineralogy and Petrology*, 89: 239-255.
- CONSTANTINO, G. & GOVETT, G.J.S. (1973): Geology, geochemistry, and genesis of Cyprus sulfide deposits. *Economic Geology*, 68: 843-858.
- COOGAN, L.A. (2003): Hidden melting signatures recorded in the Troodos ophiolite plutonic suite: evidence for widespread generation of depleted melts and intra-crustal melt aggregation. *Contributions to Mineralogy and Petrology*, 144: 484-506.
- COOGAN, L.A. & GILLIS, K.M. (2018): Temperature dependence of chemical exchange during seafloor weathering: Insights from the Troodos ophiolite. *Geochimica et Cosmochimica Acta*, 243: 24-41.
- COOGAN, L.A., GILLIS, K.M., POPE, M. & SPENCE, J. (2017): The role of low-temperature (off-axis) alteration of the oceanic crust in the global Li-cycle: Insights from the Troodos ophiolite. *Geochimica et Cosmochimica Acta*, 203: 201-215.
- COX, K.G., BELL, J.D. & PANKHURST, R.J. (1979): *The interpretation of igneous rocks*. 1. ed.; 1-450; George, Allen and Unwin, London.
- DEARING, J. (1994): *Environmental magnetic susceptibility - using the Bartington MS2 system*. 1. ed.; 1-104; Chi Publishing, Kenilworth, UK.

- DEARING, J.A., DANN, R.J.L., HAY, K., LEES, J.A., LOVELAND, P.J., MAHER, B.A. & O'GRADY, K. (1996): Frequency-dependant susceptibility measurements of environmental materials. *Geophysical Journal International*, 124: 228-240.
- DILEK, Y. & FURNES, H. (2009): Structure and geochemistry of Tethyan ophiolites and their petrogenesis in subduction rollback systems. *Lithos*, 113: 1-20.
- EBERT, Y., KESSEL, R., SHAAR, R., AGNON, A. & RON, H. (2010): Petrology and rock magnetism of the gabbro of Troodos ophiolite. *Physics of the Earth and Planetary Interior*, 183: 413-420.
- EDWARDS, S., HUDSON-EDWARDS, K., CANN, J., MALPAS, J. & XENOPHONTOS, C. (2010): Cyprus. 1. ed.; 1-271; Terra Publishing, Edinburgh.
- ELDERFIELD, H., GASS, I.G., HAMMOND, A. & BEAR, L.M. (1972): The origin of ferromanganese sediments associated with the Troodos Massif of Cyprus. *Sedimentology*, 19: 1-19.
- EVANS, M.E. & HELLER, F. (2003): Environmental magnetism - principles and applications of enviromagnetics. 1. ed.; 1-299; Academic Press, Amsterdam, Boston etc.
- FLOWER, M.F.J. & LEVINE, H.M. (1987): Petrogenesis of a tholeiite-boninite sequence from Ayios Mamas, Troodos ophiolite: evidence for splitting of a volcanic arc? *Contributions to Mineralogy and Petrology*, 97: 509-524.
- FONSECA, R.O., KIRCHENBAUR, M., BALLHAUS, C., MÜNKER, C., ZIRNER, A., GERDES, A., HEUSER, A., BOTCHARNIKOV, R. & LENTING, C. (2017): Fingerprinting fluid sources in Troodos ophiolite complex orbicular glasses using high spatial resolution isotope and trace element geochemistry. *Geochimica et Cosmochimica Acta*, 200: 145-166.
- FREUND, S., HAASE, K.M., KEITH, M., BEIER, C. & GARBE-SCHÖNBERG, D. (2014): Constraints on the formation of geochemically variable plagiogranite intrusions in the Troodos Ophiolite, Cyprus. *Contributions to Mineralogy and Petrology*, 167: 978.
- FRISCH, W. & MESCHEDÉ, M. (2005): Plattentektonik - Kontinentverschiebung und Gebirgsbildung. 1. ed.; 1-196; Primus Darmstadt.
- GILLESPIE, M.R. & STYLES, M.T. (1997): BGS rock classification scheme, Volume 1, Classification of igneous rocks. British Geological Survey Research Report, 97-2: 63+34.
- GILLIS, K.M. & COOGAN, L.A. (2002): Anatectic migmatites from the roof of an ocean ridge magma chamber. *Journal of Petrology*, 43: 2075-2095.
- GILLIS, K.M., COOGAN, L.A. & BRANT, C. (2015): The role of sedimentation history and lithology on fluid flow and reactions in off-axis hydrothermal systems: A perspective from the Troodos ophiolite. *Chemical Geology*, 414: 84-94.
- GOLOWIN, R., PORTNYAGIN, M.V., HOERNLE, K., SOBOLEV, A., KUZMIN, D. & R., W. (2017): The role and conditions of second-stage mantle melting in the generation of low-Ti

- tholeiites and boninites: the case of the Manihiki Plateau and the Troodos ophiolite. *Contributions to Mineralogy and Petrology*, 172: 1-18.
- GRANOT, R., TAUXE, L., GEE, J.S. & RON, H. (2007): A view into the Cretaceous geomagnetic field from analysis of gabbros and submarine glasses. *Earth and Planetary Science Letters*, 256: 1-11.
- GREENBAUM, D. (1977): The chromitiferous rocks of the Troodos Ophiolite Complex, Cyprus. *Economic Geology*, 72: 1175-1194.
- GRIMES, C., USHIKUBO, T., KOZDON, R. & VALLEY, J.W. (2013): Perspectives on the origin of plagiogranite in ophiolites from oxygen isotopes in zircon. *Lithos*, 179: 48-66.
- HALL, J.M., WALLS, C.C. & HALL, S.L. (1995): Viscous magnetization at 300 K in a profile through Troodos type oceanic crust *Physics of the Earth and Planetary Interior*, 88: 101-116.
- HANNINGTON, M.D., HERZIG, P.M. & ALT, J.C. (1990): The distribution of gold in sub-seafloor stockwork mineralization from DSDP hole 504B and the Agrokippa B deposit, cyprus. *Canadian Journal of Earth Sciences*, 27: 1409-1417.
- HENRY, B. (1971): Chypre: Possibilités minières et perspectives de recherches. ed.; Bureau des Recherches Géologiques et Minières, Orléans.
- HOLLOCHER, K. (2012): HGeochemistry of amphibolite-facies volcanics and gabbros of the Støren Nappe in extensions west and southwest of Trondheim, Western Gneiss Region, Norway: a key to correlations and paleotectonic settings. *American Journal of Science* 312.4, 357-416. *American J. Sci.*, 312: 357-416.
- JANOUSEK, V., FARROW, C.M. & ERBAN, V. (2006): Interpretation of whole-rock geochemical data in igneous geochemistry: introducing Geochemical Data Toolkit (GCDkit). *Journal of Petrology*, 47: 1255-1259.
- JOWITT, S.M., JENKIN, G.R.T., COOGAN, L.A. & NADEN, J. (2012): Quantifying the release of base metals from source rocks for volcanogenic massive sulfide deposits: Effects of protolith composition and alteration mineralogy. *Journal of geochemical Exploration*, 118: 47-59.
- KURZWEIL, F., MÜNKER, C., GRUPP, M., BRAUKMÜLLER, N., FECHTNER, L., CHRISTIAN, M., HOHL, S.V. & SCHOENBERG, R. (2019): The stable tungsten isotope composition of modern igneous reservoirs. *Geochimica et Cosmochimica Acta*, 251: 176-191.
- LE BAS, M.J., LE MAITRE, R.W., STRECKEISEN, A. & ZANETTIN, B. (1986): A chemical classification of volcanic rocks based on the total alkali–silica diagram. *Journal of Petrology*, 27: 745-750.
- LE MAITRE, R.W., STRECKEISEN, A., ZANETTIN, B., LE BAS, M.J., BONIN, B., BATEMAN, P., BELLINI, G., DUDEK, A., EFREMOVA, S., KELLER, J., LAMEYRE, J., SABINE, P.A., SCHMID, R., SØRENSEN, H. & WOOLLEY, A.R. (2002): *Igneous rocks - A Classification and Glossary of Terms, Recommendations of the International Union of Geological*

- Sciences Subcommittee on the Systematics of Igneous Rocks. 2. ed.; 1-236; Cambridge University Press, Cambridge, U.K.
- MACKENZIE, G.D., MAGUIRE, K.H., COOGAN, L.A., KHAN, M.A., EATON, M. & PETRIDES, G. (2006): Geophysical constraints on the crustal architecture of the Troodos ophiolite: results from the IANGASS project. *Geophysical Journal International*, 167: 1385-1401.
- MARIEN, C.S., HOFFMANN, J.E., GARBE-SCHÖNBERG, D. & MÜNKER, C. (2019): Petrogenesis of plagiogranites from the Troodos Ophiolite Complex, Cyprus. *Contributions to Mineralogy and Petrology*, 174: 35.
- MAXBAUER, D.P., FEINBERG, J.M. & FOX, D.L. (2016): Magnetic mineral assemblages in soils and paleosols as the basis for paleoprecipitation proxies: A review of magnetic methods and challenges. *Earth-Science Reviews*, 155: 28-28.
- MCPHEE, P.J. & VAN HINSBERGEN, D.J.J. (2019): Tectonic reconstruction of Cyprus reveals Late Miocene continental collision of Africa and Anatolia. *Gondwana Research*, 68: 158-173.
- MELCHER, F., MEISEL, T., PUHL, J. & KOLLER, F. (2002): Petrogenesis and geotectonic setting of ultramafic rocks in the Eastern Alps: constraints from geochemistry. *Lithos*, 65: 69-112.
- MESCHEDE, M. (1986): A method of discriminating between different types of mid-ocean ridge basalts and continental tholeiites with the Nb-Zr-Y diagram. *Chemical Geology*, 56: 207-218.
- MIDDLEMOST, E.A.K. (1989): Iron oxidation ratios, norms and the classification of volcanic rocks. *Chemical Geology*, 77: 19-26.
- MORRIS, A. & MAFFIONE, M. (2016): Is the Troodos ophiolite (Cyprus) a complete, transform fault–bounded Neotethyan ridge segment? *Geology*, 44: 199-202.
- MULLEN, E.D. (1983): MnO/TiO₂/P₂O₅: a minor element discriminant for basaltic rocks of oceanic environments and its implications for petrogenesis. *Earth and Planetary Science Letters*, 62: 53-62.
- NICOLAS, A. (1995): *Die ozeanischen Rücken - Gebirge unter dem Meer*. 1. ed.; 1-200; Springer, Berlin, Heidelberg.
- OHNENSTETTER, M., BECHON, F. & OHNENSTETTER, D. (1990): Geochemistry and Mineralogy of Lavas from the Arakapas Fault Belt, Cyprus: Consequences for Magma Chamber Evolution. *Mineralogy and Petrology*, 41: 105-124.
- OSOZAWA, S., SHINJO, R., LO, C.-H., JAHN, B.-M., HOANG, N., SASAKI, M., ISHIKAWA, K., KANO, H., HOSHI, H., XENOPHONTOS, C. & J., W. (2012): Geochemistry and geochronology of the Troodos ophiolite: An SSZ ophiolite generated by subduction initiation and an extended episode of ridge subduction? *Lithosphere*, 4: 497-510.

- PAPADOPOULOS, N.G., TSOKAS, G.N., TSOURLOS, P., CHRISTOFIDES, G. & STAMPOLIDIS, A. (2005): Analysis of the geomagnetic field and the Bouguer anomalies in Cyprus and their relation to the island's geology. *Ofioliti*, 30: 53-63.
- PATTEN, C.G.C., PITCAIRN, I.K. & TEAGLE, D.A.H. (2017): Hydrothermal mobilisation of Au and other metals in supra-subduction oceanic crust: insights from the Troodos ophiolite. *Ore geology Reviews*, 86: 487-508.
- PEARCE, J.A. (1975): Basalt geochemistry used to investigate past tectonic environments on Cyprus. *Tectonophysics*, 25: 41-67.
- PEARCE, J.A. (1976): Statistical analysis of major element patterns in basalts. *Journal of Petrology*, 17: 15-43.
- PEARCE, J.A. & MCCANN, J.R. (1973): Tectonic setting of basic volcanic rocks determined using trace element analysis. *Earth and Planetary Science Letters*, 19: 290-300.
- PEARCE, J.A. & NORRY, M.J. (1979): Petrogenetic implications of Ti, Zr, Y and Nb variations in volcanic rocks. *Contributions to Mineralogy and Petrology*, 69: 33-47.
- PEARCE, J.A. & ROBINSON, P.T. (2010): The Troodos ophiolitic complex probably formed in a subduction initiation, slab edge setting. *Gondwana Research*, 18: 60-81.
- PORTNYAGIN, M.V., DANYUSHEVSKY, L.V. & KAMENETSKY, V.S. (1997): Coexistence of two distinct mantle sources during formation of ophiolites: a case study of primitive pillow-lavas from the lowest part of the volcanic section of the Troodos Ophiolite, Cyprus. *Contributions to Mineralogy and Petrology*, 128: 287-301.
- PORTNYAGIN, M.V., SIMAKIN, S.G. & SOBOLEV, A.V. (2002): Fluorine in primitive magmas of the Troodos Ophiolite Complex, Cyprus: Analytical methods and main results. *Geochemistry International*, 40: 625-632.
- PRICHARD, H.M. & LORD, R.A. (1990): Platinum and palladium in the Troodos ophiolite complex, Cyprus. *The Canadian Mineralogist*, 28: 607-617.
- PRICHARD, H.M. & MALIOTIS, G. (1998): Gold mineralization associated with low-temperature, off-axis, fluid activity in the Troodos ophiolite, Cyprus. *Journal of the Geological Society, London*, 155: 223-231.
- RAUTENSCHLEIN, M., JENNER, G.A., HERTOGEN, J., HOFMANN, A.W., KERRICH, R., SCHMINCKE, H.-U. & WHITE, W.M. (1985): Isotopic and trace element composition of volcanic glasses from the Akaki Canyon, Cyprus: implications for the origin of the Troodos ophiolite. *Earth and Planetary Science Letters*, 75: 369-383.
- RAVIZZA, G., SHERREL, R.M., FIELD, M.P. & PICKET, E.A. (1999): Geochemistry of the Margi umbers, Cyprus, and the Os isotope composition of Cretaceous seawater. *Geology*, 27: 971-974.

- REGELOUS, M., HAASE, K.M., FREUND, S., KEITH, M., WEINZIERL, C.G., BEIER, C., BRANDL, P.A., ENDRES, T. & SCHMITDT, H. (2014): Formation of the Troodos Ophiolite at a triple junction: Evidence from trace elements in volcanic glass. *Chemical Geology*, 386: 66-79.
- REN, L., COHEN, D.R., RUTHERFORD, N.F., ZISSIMOS, A.M. & MORISSEAU, E.G. (2015): Reflections of the geological characteristics of Cyprus in soil rare earth element patterns. *Applied Geochemistry*, 56: 80-93.
- RICHARDSON, C.J., CANN, J.R., RICHARDS, H.G. & COWAN, J.G. (1987): Metal-depleted root zones of the Troodos ore-forming hydrothermal systems, Cyprus. *Earth and Planetary Science Letters*, 84: 243-253.
- ROBERTSON, A.H.F. (1973): Cyprus umbers: Chemical precipitates on a Tethyan ocean ridge. *Earth and Planetary Science Letters*, 18: 93-101.
- ROBERTSON, A.H.F. (1978): Metallogensis along a fossil oceanic fracture zone: Arakapas Fault Belt, Troodos Massif, Cyprus. *Earth and Planetary Science Letters*, 41: 317-329.
- ROBERTSON, A.H.F. & FLEET, A.J. (1976): The origins of Rare Earths in metalliferous sediments of the Troodos Massif, Cyprus. *Earth and Planetary Science Letters*, 28: 385-394.
- ROCHE, H.D.L. & LETERRIER, J. (1980): A classification of volcanic and plutonic rocks using R_1R_2 diagram and major element analysis - its relationships with current nomenclature. *Chemical Geology*, 29: 183-210.
- SALMINEN, R. (2005): *Geochemical Atlas of Europe - Part 1: Background information, methodology and maps*. 1. ed.; 1-525; Ass. Geol. Surveys European Union (EuroGeoSurveys) / Geol. Survey Finland, Helsinki.
- STRECKEISEN, A. (1973): Plutonic rocks. Classification and nomenclature recommended by the IUGS Subcommittee on the Systematics of Igneous Rocks. *Geotimes*, 18: 26-30.
- THOMPSON, R. & OLDFIELD, F. (1986): *Environmental magnetism*. 1. ed.; 1-227; Allen & Unwin, London.
- THY, P., BROOKS, C.K. & WALSH, J.N. (1985): Tectonic and petrogenetic implications of major and rare earth element chemistry of Troodos glasses, Cyprus. *Lithos*, 18: 165-178.
- TRÖGER, W.E., BAMBAUER, H.U., TABORSZKY, F. & TROCHIM, H.D. (1982): *Optische Bestimmung der gesteinsbildenden Minerale, Teil 1 Bestimmungstabellen*. 5. ed.; 1-188; Schweizerbart, Stuttgart.
- VARGA, R.J., GEE, J.S., BETTISON-VARGA, L., ANDERSON, R.S. & JOHNSON, C.L. (1999): Early establishment of seafloor hydrothermal systems during structural extension: paleomagnetic evidence from the Troodos ophiolite, Cyprus. *Earth and Planetary Science Letters*, 171: 221-235.

- VINE, F.J., POSTER, C.K. & GASS, I.G. (1973): Aeromagnetic survey of the Troodos igneous massif, Cyprus. *Nature Physical Science* 244: 34-38.
- WILSON, M. (1989): *Igneous petrogenesis - a global tectonic approach*. 1. ed.; 1-466; Chapman & Hall, London, etc.
- WIMMENAUER, W. (1985): *Petrographie der magmatischen und metamorphen Gesteine*. 1. ed.; 1-382; Enke Verlag, Stuttgart.
- WINCHESTER, J.A. & FLOYD, P.A. (1976): Geochemical magma type discrimination application to altered and metamorphosed basic igneous rocks *Earth and Planetary Science Letters*, 28: 459-469.
- WÖLKI, D., P., M., REGELOUS, M. & HAASE, K. (2019): Enrichment of H₂O and fluid-soluble trace elements in the Troodos Ophiolite: Evidence for a near-trench origin. *Lithos*, 1-12.
- WÖLKI, D., REGELOUS, M., HAASE, K.M. & BEIERA, C. (2019): Geochemical mapping of a paleo-subduction zone beneath the Troodos Ophiolite. *Chemical Geology*, 523: 1-8.
- WÖLKI, D., REGELOUS, M., HAASE, K.M., ROMER, R.H.W. & BEIER, C. (2018): Petrogenesis of boninitic lavas from the Troodos Ophiolite, and comparison with Izu–Bonin–Mariana fore-arc crust. *Earth and Planetary Science Letters*, 498: 203-214.
- WOOD, D.A., JORON, J.L. & TREUIL, M. (1979): A re-appraisal of the use of trace elements to classify and discriminate between magma series erupted in different tectonic settings. *Earth and Planetary Science Letters*, 45: 326-336.